ELSEVIER

Coordination Chemistry Reviews
208 (2000) 331–364

COORDINATION CHEMISTRY REVIEWS

www.elsevier.com/locate/ccr

Triplets in metal–organic compounds. Chemical tunability of relaxation dynamics

Hartmut Yersin *, Johann Strasser

Institut für Physikalische und Theoretische Chemie, Universität Regensburg, D-93040 Regensburg, Germany

Received 16 November 1999; accepted 23 February 2000

Contents

* Corresponding author. Tel.: +49-941-9434464; fax: +49-941-9434488.
E-mail address: harmut.yersin@chemie.uni-regensburg.de (H. Yersin).

PII: S0010-8545(00)00326-X

Abstract

Triplets of metal–organic or related compounds of the platinum metal group split into substates. The amount of splitting at zero magnetic field (zfs) is mainly determined by the effective spin-orbit coupling, which is, for example, induced by metal-d and/or MLCT participations in these triplets. The total zfs can be tuned chemically over a very wide range from about 0.1 cm^{-1} to more than 200 cm^{-1} (see Fig. 1). After excitation, the relaxation time between the substates can be as long as hundreds of nano-seconds to many micro-seconds at low temperature. This relaxation, the spin-lattice relaxation (slr), depends on the splitting pattern of the triplet substates, further on temperature, and on the matrix surrounding the chromophore. Four compounds $[Pt(bpy)_2]^{2+}$, Pt(2-thpy)(CO)(Cl), $Pt(2\text{-thpy})_2$, and $[Ru(bpy)_3]^{2+}$ with strongly different zero-field splittings are selected as case studies, to investigate the dynamics of slr according to the direct, the Orbach, and the Raman process. Temperature dependent studies and investigations at low temperature ($T \leq 2$ K) under application of high magnetic fields up to $B = 10$ T and high pressure up to $p = 20$ kbar, respectively, allow us to develop a deeper insight into the relaxation mechanisms. Moreover, several effects are pointed out that result from slow spin-lattice relaxation and that can be important at low temperature, like the non-validity of a Boltzmann distribution for closely lying states, the occurrence of super-imposed emission spectra from different excited states, the dependence of emission decay properties on excitation and detection wavelengths, effects of spectral shifts with time, and a specific behavior of radiationless energy transfer. In an outlook, a number of further transition metal complexes is presented to underline the general importance of the effects of relatively slow spin-lattice relaxation.

Keywords: Metal–organic compounds; Chemical tunability; Relaxation dynamics; Spin-lattice relaxation (slr); Zero-field splitting

1. Introduction

Ions of the platinum metal group can form a very large number of complexes by coordinating with different organic ligands. Thus, it is feasible to select series of compounds with specific properties. For example, one can choose a series, in which the character of the lowest excited state(s) can systematically be varied from largely ligand-centered (LC) to metal-to-ligand-charge-transfer (MLCT) character. This is possible due to an increase of metal-d participation in these states [1–3]. The amount of metal admixture is of particular importance for the lowest emitting triplet states. (Mostly, the lowest excited states are triplets, while the ground states are singlets.) Thus, in such a series, the zero-field splittings (zfs) of the triplets, the transition probabilities between triplets and ground states, the emission decay times, efficiencies of energy transfer, etc. can vary by orders of magnitude [1–3]. Also other properties exhibit strong systematic changes, like spatial extensions of the lowest excited states, changes of binding properties or vibrational force constants upon excitation, etc. [1–6].

In the present investigation it is intended to focus on dynamical processes, which govern the populations of the lowest triplet sublevels. These populations are

essentially determined by the times of relaxation between the different spin-substates. These relaxation times can be very long at low temperatures, when the energy separations between the substates are of the order of several wavenumbers or less. This behavior is related to the fact that the excess energy of a higher triplet sublevel is not easily transferred to the lattice (or matrix) due to the small density of states of lattice vibrations in this energy range and due to the requirement of spin-flips for transitions between these substates. This type of relaxation is called spin-lattice relaxation (slr). Although, it is known since decades that such slow processes are significant (e.g. see the Refs. [7–15]), the almost general importance of these effects also for metal–organic compounds has not yet been fully recognized. Three processes are important and govern the relaxation properties between closely lying electronic states, namely the direct, the Orbach, and the Raman process (see Refs. [10–15] and below). These processes or the corresponding rates determine many properties at low temperatures, like emission spectra [16,17], emission decay times [18–20], rates of radiationless energy transfer [21–23], and probably also rates of photochemical reactions, when the triplets are involved.

The importance of the different slr processes depends strongly on the specific size and pattern of zero-field splitting of a triplet. Recently, it has been shown that the total zfs for the type of compounds discussed here is correlated to the metal participation in the triplet wavefunctions. Thus, one obtains a relation, as presented in Fig. 1. The significance and validity of such a relation involving bpy-compounds and *cyclo*-metalated Pt-complexes has thoroughly been justified in Refs. [1] and [6].

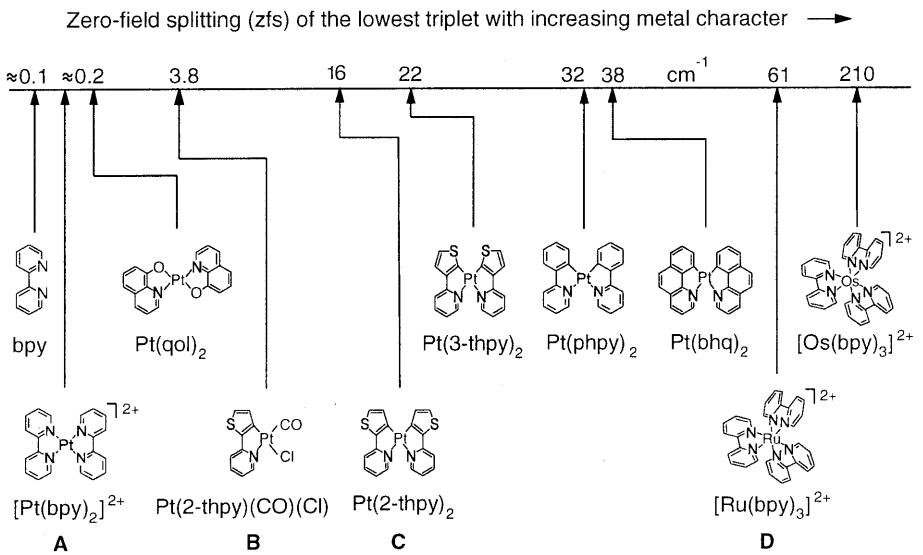

Fig. 1. The diagram symbolizes the significance of metal character for the lowest triplet. The corresponding metal admixture correlates with the total splitting of the triplet at zero magnetic field (zfs). Properties of the compounds **A**, **B**, **C**, and **D** are presented in detail as case studies.

It is the subject of the present investigation, to use the possibility of chemically tuning the amount of zfs (or of the metal participation). This is demonstrated by presenting four case studies **A**, **B**, **C**, and **D**, which display different situations with regard to the dynamical behavior of the spin-lattice relaxation. It is also shown that the corresponding rates or times of spin-lattice relaxation can additionally be tuned physically by changing temperature, magnetic fields, and/or by applying high pressure.

The paper is organized as follows: In Section 2, the different processes of spin-lattice relaxation are sketched. Although some theoretical expressions are used in this section, the case studies presented in Section 3 will be discussed in a way, which allows a relatively easy reading. These case studies are arranged according to an increasing zero-field splitting. In **Case Study A**, the $[Pt(bpy)_2]^{2+}$ compound with zfs of the order of 0.1 cm^{-1} is investigated at $T = 1.3$ K. **Case Study B** presents properties of **Pt(2-thpy)(CO)(Cl)** (zfs: 3.8 cm^{-1}) under variation of temperature, and in **Case Study C**, slr properties of **$Pt(2\text{-thpy})_2$** (zfs: 16 cm^{-1}) are discussed under variation of temperature and high magnetic fields. In **Case Study D**, the situation is examined for $[Ru(bpy)_3]^{2+}$ (zfs: 61 cm^{-1}), by studying slr properties as functions of temperature and high pressure. Finally, the paper is concluded by a short summary and outlook.

2. Processes of spin-lattice relaxation

At low temperature, a relaxation from an electronically excited state of a molecule to a lower lying excited state can be very slow, when the energy separation between these two states lies in the order of several cm^{-1} or lower. This situation occurs usually for zero-field split triplet sublevels. The smallness of the rate of spin-lattice relaxation is a consequence of the fact that the density of states of lattice or phonon modes in this energy range is usually very small. Thus, the excess energy of the chromophore is not easily transferred to the lattice. Further, a relaxation from one triplet substate to another one requires a spin-flip, which additionally reduces the relaxation rate(s). In the literature, different mechanisms have been discussed, which may induce a spin-flip due to an interaction of phonons with the triplet sublevels of the molecule (e.g. see [8–15,24,25]). Important is that phonon modes can cause fluctuations of molecular properties, like intramolecular distances, and thus can modulate the electronic charge distributions, spin-orbit coupling, mixing coefficients between different states, etc. However, it is not in the scope of the present investigation to discuss these mechanisms. Here, we only take into account that a perturbation V caused by the phonons can couple the electronic states $|a\rangle$ and $|b\rangle$ (triplet substates) of the chromophore (Fig. 2).

A description of the temperature dependence of the rates of spin-lattice relaxation is usually based on the consideration of the three different processes, which are schematically sketched in Fig. 2. $|a\rangle$, $|b\rangle$, and $|c\rangle$ represent, for example, the three triplet sublevels $|I\rangle$, $|II\rangle$, and $|III\rangle$ split by several cm^{-1}. It is assumed that one of the higher lying states, say $|b\rangle$, is populated by a relaxation from a still

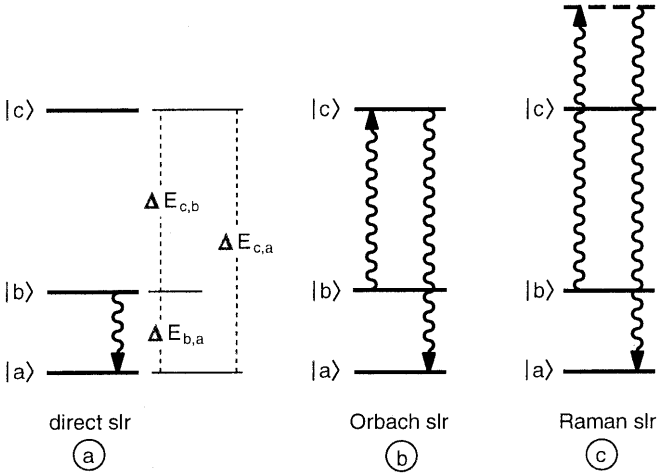

Fig. 2. Schematic diagram to introduce the processes of spin-lattice relaxation (slr). The states $|a\rangle$, $|b\rangle$, and $|c\rangle$ represent, for example, triplet substates of metal–organic compounds. The corresponding zero-field splittings lie in the energy range from 0.1 to about 10^2 cm^{-1}.

higher lying state (for example by a process of intersystem crossing from S_1) or by an excitation of just this electronic state.

2.1. Direct process

A relaxation from state $|b\rangle$ to state $|a\rangle$ may occur by an emission of just one phonon with the energy $\Delta E_{b,a}$, which is transmitted to the lattice. This process is called direct process of spin-lattice relaxation. The corresponding rate $k_{b,a}^{\mathrm{slr}}$ (direct) is usually dominant at low temperature T and exhibits only a weak temperature dependence. For this rate one obtains (e.g. see the Refs. [10,14,15,26,27]):

$$k_{b,a}^{\mathrm{slr}}(\mathrm{direct}) = \frac{3}{2\pi\hbar^4\rho v^5} \cdot |\langle b|V|a\rangle|^2 \cdot (\Delta E_{b,a})^3 \cdot \coth(\Delta E_{b,a}/2k_{\mathrm{B}}T) \quad (1)$$

Here, ρ is the mass density of the matrix material, v the (average) velocity of sound of the matrix, and k_{B} the Boltzmann constant.

2.2. Orbach process

With temperature increase, the relaxation may also proceed indirectly by the two phonon Orbach process (Fig. 2b). Schematically, in this process, one phonon of the energy $\Delta E_{c,b}$ is absorbed, while a second phonon of the energy $\Delta E_{c,a}$ is emitted. The rate of this process has been determined recently also for a general pattern of zero-field splitting, as one finds often for the compounds being of interest here. The general result is presented in Ref. [[26] Eq. (16)]. Here, we use a slightly simplified low-temperature approximation [26]:

$$k_{b,a}^{\mathrm{slr}}(\mathrm{Orbach}) = \frac{C_{c,b}C_{c,a}(e^{\Delta E_{c,b}/k_B T} + e^{\Delta E_{c,a}/k_B T})}{C_{c,a}e^{\Delta E_{c,a}/k_B T}(e^{\Delta E_{c,b}/k_B T} - 1) + C_{c,b}e^{\Delta E_{c,b}/k_B T}(e^{\Delta E_{c,a}/k_B T} - 1)} \quad (2)$$

with the abbreviations

$$C_{c,a} = \frac{3}{2\pi\hbar^4\rho v^5}|\langle c|V|a\rangle|^2 \cdot (\Delta E_{c,a})^3 \quad (3)$$

$$C_{c,b} = \frac{3}{2\pi\hbar^4\rho v^5}|\langle c|V|b\rangle|^2 \cdot (\Delta E_{c,b})^3$$

$$C_{b,a} = \frac{3}{2\pi\hbar^4\rho v^5}|\langle b|V|a\rangle|^2 \cdot (\Delta E_{b,a})^3$$

All parameters or matrix elements used are defined above or correspond directly to the definitions given. The energy separations are specified in Fig. 2.

From the general Eq. (2) one can obtain the original Orbach expression, which was derived under the assumption of the specific energy differences $\Delta E_{c,a} \approx \Delta E_{c,b} = \Delta E$ (e.g. see Refs. [10–12,14,15]):

$$k_{b,a}^{\mathrm{slr}}(\mathrm{Orbach}) \approx \frac{2C_{c,b}C_{c,a}}{(C_{c,a} + C_{c,b})} \cdot \frac{1}{e^{\Delta E/k_B T} - 1} \quad (4)$$

This expression can further be simplified for $\exp(\Delta E/k_B T) \gg 1$ or $\Delta E \gg k_B T$. Thus, one obtains

$$k_{b,a}^{\mathrm{slr}}(\mathrm{Orbach}) \approx \mathrm{const} \cdot (\Delta E)^3 \cdot e^{-\Delta E/k_B T} \quad (5)$$

This simple approximation has, for example, successfully been used to fit the temperature dependence of the spin-lattice relaxation rate of $[Ru(bpy)_3]^{2+}$ doped into $[Zn(bpy)_3](ClO_4)_2$ up to $T \approx 10$ K. (See Ref. [1] and Section 3.4.2.)

For completeness it is mentioned that the rate according to the Orbach process vanishes for $T \to 0$ K and also for $\Delta E \to 0$ cm^{-1}.

2.3. Raman process

In addition to the processes (a) and (b) a two-phonon Raman scattering process can also lead to a relaxation from state $|b\rangle$ to state $|a\rangle$ according to Fig. 2c. The temperature dependence of the respective rate is usually approximated by [10,13,14,28]:

$$k_{b,a}^{\mathrm{slr}}(\mathrm{Raman}) = R \cdot T^n \quad (6)$$

with a constant R and $n = 5$ or $n = 7$ for non-Kramers ions [13]. For the compounds studied here, the T^5 dependence fits the experimental observations much better than the T^7 dependence observed for other systems [10,29]. (See also below.)

3. Relaxation behavior in the system of triplet substates

The relaxations, which occur between the triplet substates of metal–organic or related complexes, depend strongly on the sizes and individual patterns of zfs. In

this section, four case studies are presented, by discussing different complexes of the platinum metal group. These complexes are selected in particular with respect to an increasing metal character in the lowest excited triplet states (see Fig. 1). As consequence of the resulting zfs patterns one observes extremely different relaxation properties at low temperatures.

3.1. Case study A: $[Pt(bpy)_2]^{2+}$

The metal character in the lowest triplet of $[Pt(bpy)_2]^{2+}$ is very small [1–3,20]. Thus, the zero-field splitting lies in the order of 0.1 cm^{-1} and therefore, in some respects the properties of spin-lattice relaxation are similar to those of organic compounds. $[Pt(bpy)_2]^{2+}$ has been investigated spectroscopically as energetically low-lying trap in $[Pt(bpy)_2](ClO_4)_2$ single crystals. By this technique, one obtains highly resolved emission and excitation spectra of one single site (fwhm ≈ 4 cm^{-1}). While for the emission the spectral range is not restricted, well defined one-site excitation spectra can only be recorded in a spectral range of about 50 cm^{-1}, since at higher energy relative to the electronic origin of this low-lying trap, one finds the majority of absorbing chromophores. Nevertheless, an analysis of the lowest excited triplet is possible [1,2,20]. This triplet is mainly of bpy $\pi\pi^*$ ligand character, but the state exhibits a small amount of metal-to-ligand-charge transfer (^{1}MLCT) admixture. Thus, due to the larger spin-orbit coupling compared to organic compounds the transition between the singlet ground state S_0 and the triplet state T_1 is observable in emission and in excitation (absorption) spectra. The electronic origin (0–0 transition) of the $S_0 \leftrightarrow T_1$ transition is found at 21 237 cm^{-1} (Fig. 3). Due to the still small admixture of metal character, the splitting of T_1 into the three triplet sublevels is very small and cannot be resolved by the optical methods applied in this investigation. Presumably, the splitting at zero magnetic field lies in the range of 0.1–0.2 cm^{-1} (3 to 6 GHz). An application of a high magnetic field, for example of $B = 7$ T, shows a splitting into the three triplet sublevels (Zeeman components) [1]. At this field strength, the total splitting is ≈ 14 cm^{-1} and thus corresponds to a g-value of two. This value is typical for spin triplets in the high-field limit.

In the context of this section, we mainly focus on the decay behavior of the triplet. Usually, this behavior depends on the excitation wavelength. After an excitation into a higher lying state (e.g. $S_0 \rightarrow S_1$, for a different excitation wavelength see below), the intersystem crossings to the three triplet sublevels are relatively fast (order of ps, e.g. compare Ref. [18]). They are populated individually, and usually, at low temperature (e.g. at $T = 1.3$ K), they are not in a fast thermal equilibrium. This is a consequence of the fact that all rates of spin-lattice relaxation, as discussed in Section 2, become very small for energy separations of the order of 0.1 cm^{-1} and at low temperature. For example, the relaxation time between the three substates according to the direct process has been estimated to be of the order of one second at $T = 1.3$ K for a different but comparable compound [26]. (Compare also Ref. [29]). It follows that during the time, the triplet is populated, effects of thermalization can be neglected. Therefore, all three sublevels emit according to their individual decay times. For $[Pt(bpy)_2]^{2+}$, the values correspond-

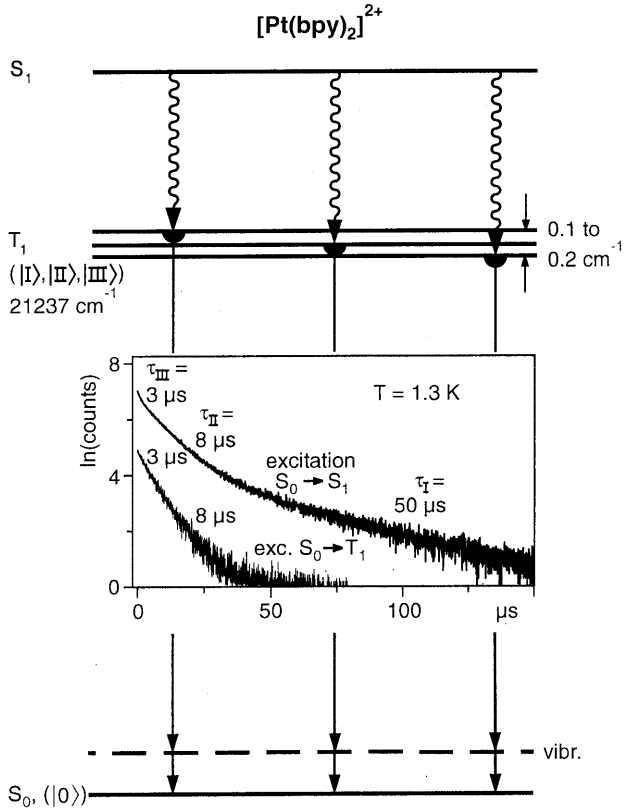

Fig. 3. Energy level scheme and emission decay properties of $[Pt(bpy)_2]^{2+}$ as trap in $[Pt(bpy)_2](ClO_4)_2$. At low temperature ($T = 1.3$ K), the emission decay depends on the excitation energy as is specified in the inset. (Results from Refs. [20,41].)

ing to the three triplet substates $|I\rangle$, $|II\rangle$, and $|III\rangle$ are determined to $\tau_I = 50$ µs, $\tau_{II} = 8$ µs, and $\tau_{III} = 3$ µs, respectively (Fig. 3). In particular, the occurrence of these three decay components demonstrates the existence of the three substates also at zero magnetic field. Thus, the time resolution gives an insight into properties of the triplet state, although the substates are spectrally not resolved. It is even possible to measure individual spectra from the different substates by use of methods of time-resolved spectroscopy, as has been demonstrated in Ref. [2] for $[Pt(bpy)_2]^{2+}$ and in more detail in Ref. [17] for the related $Pd(2\text{-thpy})_2$ compound.

For completeness, it is mentioned that the behavior described is in many respects very similar to the one found for organic compounds, as has been reported already decades ago [29,31,32]. Moreover, the non-thermalization at low temperature is the basis of the important method of optically detected magnetic resonance (ODMR) [33–35]. This and related methods have not only been applied to organic molecules but also to metal–organic and related compounds of the platinum metal group (e.g. see Refs. [30,36–40]).

Interestingly, for many transition metal compounds the transition probability of $S_0 \rightarrow T_1$ is large enough to excite the triplet directly, which, usually, is not easily achievable for organic molecules. For $[Pt(bpy)_2]^{2+}$, the corresponding excitation is possible, when the excitation energy of 21 237 cm^{-1} is chosen. However, one of the three triplet substates, namely the long-living state $|I\rangle$, does not absorb sufficiently. Consequently, only the two other substates $|II\rangle$ and $|III\rangle$ are significantly populated by a short laser pulse. Since the thermalization between the three states may be neglected at $T = 1.3$ K, one observes only a bi-exponential emission decay with the two decay components of $\tau_{II} = 8$ μs and $\tau_{III} = 3$ μs [41] (Fig. 3).

With temperature increase (e.g. $T > 5$ K), when the rates of spin-lattice relaxation become larger and the thermalization becomes fast, the individual decay components are no longer observable. This leads to an average mono-exponential emission decay, which can be expressed by the three low-temperature values (e.g. see [31]).

$$\tau_{av} = 3(1/\tau_I + 1/\tau_{II} + 1/\tau_{III})^{-1} \quad (7)$$

For $[Pt(bpy)_2]^{2+}$, one obtains formally a value of $\tau_{av} = 6.3$ μs. But experimentally, this mono-exponential decay could not be determined for the investigated $[Pt(bpy)_2]^{2+}$ trap in neat $[Pt(bpy)_2](ClO_4)_2$, since at higher temperatures, like $T > 5$ K, energy transfer processes between different traps become important and thus a number of additional deactivation channels are opened. However, the described behavior has been verified for several other transition metal compounds, as for $[Rh(bpy)_3]^{3+}$ [1–3], $Pd(2\text{-thpy})_2$ [17], and $Pt(qol)_2$ [18,42].

The processes of spin-lattice relaxation, which become important with temperature increase, have not yet been investigated in the literature for transition metal complexes with zfs of the order of $\Delta E = 0.1$ cm^{-1}. However, it can be concluded that according to the $(\Delta E)^3$ dependence of the direct process (Eq. (1)) this rate will certainly not be significant. The same conclusion is also valid for the Orbach process (Eqs. (2) and (3)), if no further electronic state is present in an energy range of about a hundred wavenumbers above the three triplet sublevels. (Compare Ref. [26] and Case Studies C and D.) Interestingly, the investigations carried out in Case Study B indicate the significance of the Raman process for higher temperatures.

3.2. Case study B: Pt(2-thpy)(CO)(Cl)

Pt(2-thpy)(CO)(Cl) represents a compound, for which the zero-field splitting of the triplet is at least by a factor of twenty larger than for $[Pt(bpy)_2]^{2+}$ due to a higher metal admixture to the lowest triplet. Important is that the resulting splitting of 3.8 cm^{-1} can optically be well resolved (Fig. 4). The greater metal admixture becomes also obvious from comparisons of the vibrational satellite structures, maximum Huang Rhys factors, etc. (not discussed in detail, but see Ref. [43]). Nevertheless, the triplet substates may still be assigned to be mainly of (2-thpy)-ligand-centered (LC) character, which however, are distorted by some MLCT admixtures. (Compare also the systematics presented in Refs. [1–4,6] and the detailed argumentation carried out for $Pt(2\text{-thpy})_2$ in Ref. [44].) In conclusion and with regard to the sequence presented in Fig. 1, one can use Pt(2-thpy)(CO)(Cl) as a

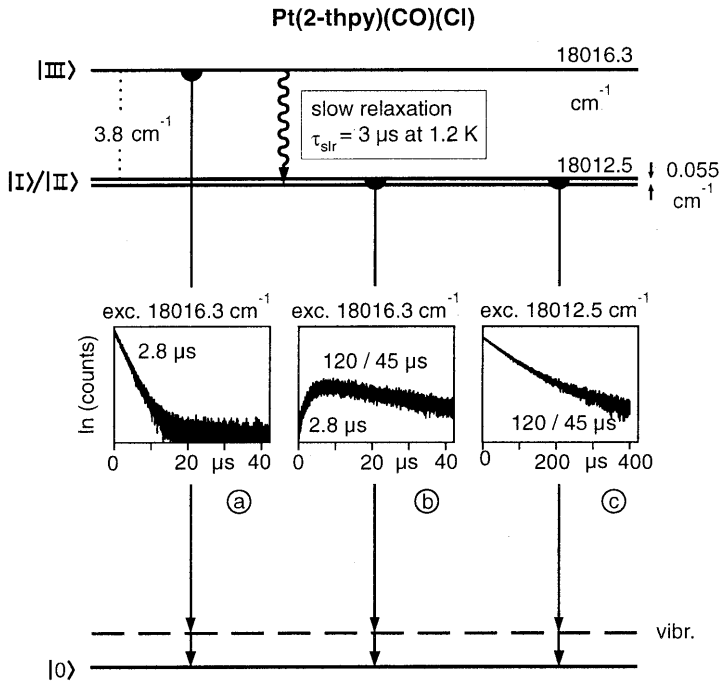

Fig. 4. Triplet sublevels of Pt(2-thpy)(CO)(Cl) and emission decay and rise behavior at $T = 1.2$ K in an *n*-octane matrix. The zero-field splitting of the states $|I\rangle$ and $|II\rangle$ is determined by ODMR measurements [47].

representative, for which the metal admixture has chemically been 'tuned' to a larger amount compared to $[Pt(bpy)_2]^{2+}$. This opens access to a detailed insight into the relaxation dynamics. In particular, the specific pattern of zero-field splitting is responsible for the significance of the direct process of slr at low temperature and the increasing importance of the Raman process with growing temperature.

Pt(2-thpy)(CO)(Cl) has been investigated in an *n*-octane matrix, a so-called Shpol'skii matrix [45], with a concentration of about 10^{-5} mol l^{-1}. This crystalline matrix is comparatively inert with respect to chromophore-matrix interactions (e.g. see Ref. [46]) and therefore it is very well suited for spectroscopic investigations also of transition metal compounds. However, the dopants should be neutral, nearly planar, and exhibit a relatively small dipole moment in the electronic ground state. (For example, see the Refs. [4,6,16–19,26,30,39–47]). These conditions are sufficiently well fulfilled for Pt(2-thpy)(CO)(Cl). Thus, by using the methods of site-selective and line-narrowing spectroscopy one obtains highly resolved spectra (fwhm < 2 cm^{-1}), which show the electronic origins and the corresponding vibrational satellite structures in emission and in excitation spectra [43]. This information allows us, to obtain a deep insight into the electronic and vibrational structures of the electronic ground state and the lowest excited and emitting triplet [19,26,43]. These optical experiments reveal at zero magnetic field only two electronic origins

of the triplet, which are separated by 3.8 cm^{-1} (Fig. 4). However, the missing third triplet sublevel is easily found under application of a high magnetic field of $B = 12$ T, namely the lowest origin at 18 012.5 cm^{-1} splits by ≈ 10 cm^{-1}. Independently, ODMR experiments at zero magnetic field show that the two lowest triplet substates are split by 1.646 GHz (0.055 cm^{-1}) [47].

3.2.1. Decay properties at low temperature

Due to the different pattern of zfs of Pt(2-thpy)(CO)(Cl) compared to the pattern presented in Case Study A, one obtains a completely different emission decay behavior of the triplet substates (Fig. 4). A resonant excitation at $\bar{\nu}_{exc} = 18\ 016.3$ cm^{-1} ($|0\rangle \rightarrow |III\rangle$) with a short laser pulse gives a mono-exponential emission decay of $\tau_{exp} = 2.8$ μs ($T = 1.2$ K) at least for five decay times. However, this is only valid, if the emission is detected on one of those specific vibrational satellites, which belong to the emission spectrum of this substate $|III\rangle$ (e.g. electronic origin $|III\rangle \rightarrow |0\rangle$ at 18 016.3 cm^{-1} minus 714.5 cm^{-1} vibration = 17 301.8 $cm^{-1} = \bar{\nu}_{det}$) (Fig. 4a). The value of $\tau_{exp} = 2.8$ μs is much shorter, than the time of emission decay from state $|III\rangle$ to the electronic ground state $|0\rangle$ of $\tau_{III} = 35$ μs. This value is not observed directly. However, it can be determined from the temperature dependence of the emission decay, when the thermal equilibration between the triplet sublevels is attained [26]. (Compare also Refs. [48,49].) Therefore, the measured decay time of $\tau_{exp} = 2.8$ μs (at $T = 1.2$ K) is assigned to be dominantly (see below, Eq. (8)) determined by emissions of phonons with the energy of 3.8 cm^{-1}, which corresponds to the energy difference from state $|III\rangle$ to the states $|I\rangle$ and $|II\rangle$. The phonons are absorbed by the lattice. These processes representing direct processes of spin-lattice relaxation (Fig. 2a), lead to the populations of the lower lying states $|I\rangle$ and $|II\rangle$. Indeed, the corresponding emission rise can also be observed (Fig. 4b), when the detection energy is correctly chosen, for example to $\bar{\nu}_{det} = 18\ 012.5$ cm^{-1}, whereby the excitation energy is not altered. In particular, this behavior represents a clear demonstration of the occurrence of a slr process.(See also Ref. [19].)

For this compound, it is also possible to excite both lower lying triplet sublevels $|I\rangle$ and $|II\rangle$ by use of an excitation energy of $\bar{\nu}_{exc} = 18\ 012.5$ cm^{-1}. If the detection is carried out on one of those specific vibrational satellites that belong to the emissions from these two states $|I\rangle$ and $|II\rangle$ (e.g. at $\bar{\nu}_{det} = 18\ 012.5–714.5$ $cm^{-1} =$ 17298 cm^{-1}), one observes the usual emission decay components of these two states with $\tau_I = 120$ μs and and $\tau_{II} = 45$ μs [19] (Fig. 4c). Presumably, the thermalization time between these closely lying states $|I\rangle$ and $|II\rangle$ (split by 0.055 cm^{-1} [47]) is – as discussed in Case Study A – much longer than the corresponding emission decay times. Therefore, one can observe both decay components.

The measured emission decay time of $\tau_{exp} = 2.8$ μs corresponding to the rate of $k_{exp} = 3.6 \times 10^5$ s^{-1} (detected in the emission spectrum of state $|III\rangle$, Fig. 4a) is not exactly the slr rate, since the experimental value is slightly shortened by the radiative and non-radiative decays from state $|III\rangle$ to the electronic ground state $|0\rangle$. The corresponding rate is $k_{III} = 2.86 \times 10^4$ s^{-1} ($k_{III} = 1/\tau_{III} = 1/35$ μs [26]). With this value, one obtains the rate of spin-lattice relaxation

$$k^{slr} = k_{exp} - k_{III} \quad (8)$$

The corrected value is determined to k^{slr} ($T = 1.2$ K) $= 3.3 \times 10^5$ s^{-1}. This rate corresponds to the slr time of $\tau = 3.0$ μs, as is marked in Fig. 4.

At very low temperature, the Orbach and the Raman process do not give any significant contributions to the slr. Therefore, the effective process of slr at $T = 1.2$ K is a direct process. However, the rate given in Eq. (1) must be slightly modified, since one has to take into account that the total rate results from two relaxation processes, namely of slr from state $|III\rangle$ to state $|I\rangle$ and to state $|II\rangle$. In Ref. [26] it is shown that under assumption of reasonable values for the mass density ($\rho \approx 0.9$ g cm^{-3}, determined from the crystal structure of *n*-octane [50]) and the velocity of sound (value of the comparable matrix cyclohexane, $v \approx 1.3$ km s^{-1} [29,51]) and by using emission decay properties that are obtained after selective excitation, one can estimate the absolute values of the matrix elements $|\langle III|V|I\rangle|$ and $|\langle III|V|II\rangle|$ to about 0.8 and 1 cm^{-1}, respectively. These values indicate that the phonon-induced couplings between the corresponding states are relatively small.

3.2.2. Temperature dependence and Raman process

With increasing temperature, the rates of spin-lattice relaxation for the processes from state $|III\rangle$ to the two lower lying states $|I\rangle$ and $|II\rangle$ increase. The experimental data, shown in Fig. 5, are determined from the emission decay values of state $|III\rangle$ under consideration of Eq. (8). These data can be well fitted by only taking into

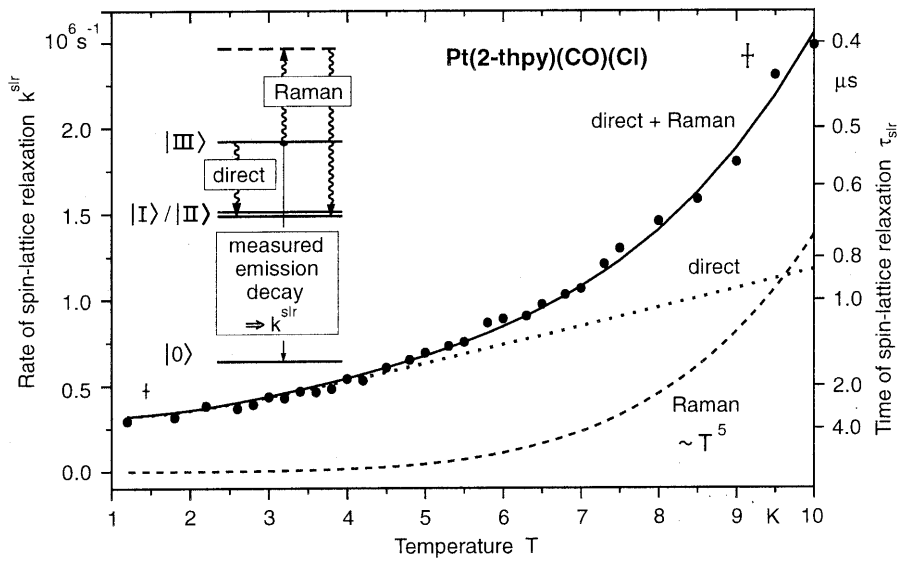

Fig. 5. Temperature dependence of the rate (and time) of spin-lattice relaxation for the processes from state $|III\rangle$ to the states $|I\rangle$ and $|II\rangle$ of Pt(2-thpy)(CO)(Cl) in *n*-octane. The solid line represents a fit according to Eq. (9), while the dotted and the broken lines give the contributions of the respective processes. (Compare also Ref. [26].) The crosses give estimated experimental errors. The inset shows the energy level diagram and symbolizes the relevant processes of spin-lattice relaxation.

account direct processes (Eq. (1)) and Raman processes (Eq. (6)) of slr. By identifying state $|b\rangle$ of Eq. (1) with state $|III\rangle$ and state $|a\rangle$ with $|I\rangle$ and $|II\rangle$, respectively, one obtains

$$k^{slr}(T) = C_1 \cdot (\Delta E)^3 \cdot \coth(\Delta E/2k_B T) + R \cdot T^5 \quad (9)$$

The value $\Delta E = \Delta E_{III,I} \approx \Delta E_{III,II} \approx 3.8\ cm^{-1}$ is known from highly resolved spectra and C_1, being given by the sum of two processes, represents those parameters, which are (nearly) independent of temperature. From Eq. (1), C_1 can be calculated by use of the low-temperature value of k^{slr}. One obtains $C_1 = 5.9 \times 10^3\ s^{-1}\ cm^3$. Thus, only one free parameter R has to be determined by the fitting procedure [52]. One finds $R = (15 \pm 3)\ s^{-1}\ K^{-5}$. Interestingly, if one additionally allows a free fit of the exponent n of the T^n power law (Eq. (6)), which describes the Raman process, one obtains $n = (4.8 \pm 0.3)$. Moreover, a function, which explicitly assumes a T^7 dependence, does not fit the experimental data. Consequently, the Raman processes, which are effective in this situation, are well characterized by a T^5 power law.

Moreover, an explicit consideration of an Orbach process has also been carried out. Due to the fact that no further electronic states are present in the corresponding energy range [19,26], it may be assumed that a localized phonon state is active as intermediate state (e.g. the 11 cm^{-1} phonon [43]). However, the inclusion of this process does not improve the fit described by Eq. (9) (Fig. 5). Obviously, the Orbach process is not of importance for the spin-lattice relaxation from state $|III\rangle$ to the two states $|I\rangle$ and $|II\rangle$ in Pt(2-thpy)(CO)(Cl). This behavior is different from the situations found for $Pt(2\text{-thpy})_2$ in *n*-octane and $[Ru(bpy)_3]^{2+}$ doped into $[Zn(bpy)_3](ClO_4)_2$ (see below). For these latter compounds real electronic states are active as intermediate states.

In Fig. 5, the temperature dependences of both relevant processes of slr are also plotted separately. Thus, the results show that up to $T \approx 5$ K, only the direct process is effective, while at higher temperature the slr according to the Raman process grows in and becomes dominant near $T = 10$ K.

3.3. Case study C: $Pt(2\text{-thpy})_2$

$Pt(2\text{-thpy})_2$ has been prepared at first by A. von Zelewsky's group and has become attractive due to many interesting photochemical and photophysical properties [4,6,16,19,26,27,44,46,53–56]. With respect to the present investigation, it is selected, since the metal character of the lowest triplet is significantly larger than for both compounds discussed above (Compare Fig. 1). Consequently, the pattern and the size of total zero-field splitting become very different. It will be shown by use of the temperature dependence of the relaxation dynamics that all three processes of spin-lattice relaxation are important, namely the direct, the Orbach, and the Raman process. Moreover, $Pt(2\text{-thpy})_2$ shows very specific slr effects under application of high magnetic fields.

Detailed information about the lowest triplet and the singlet ground state of $Pt(2\text{-thpy})_2$ could be obtained, when the compound was dissolved in an n-octane

Shpol'skii matrix [4,6,16,19,26,27,44,46]. Emission and excitation measurements allowed us to determine the energy level diagram for the three triplet sublevels (Fig. 6). Moreover, the triplet could be classified as being mainly of $^3\pi\pi^*$-ligand character, which is significantly distorted by an MLCT admixture. (See the Refs. [1,4,44], Fig. 1 and compare Ref. [56].) Due to the metal contribution, the total zfs becomes relatively large (16 cm^{-1}) and, interestingly the two ligands are sufficiently coupled electronically (metal-mediated) to delocalize the three triplet sublevels over both ligands [6].

3.3.1. Emission decay properties at low temperature

For $Pt(2\text{-thpy})_2$, the energy differences between the three triplet sublevels are nearly equal (Fig. 6). Thus, it becomes particularly interesting to study the relaxation behavior of state $|II\rangle$ after a pulsed excitation of this state (e.g. $\bar{\nu}_{exc}$:$|0\rangle \rightarrow |II\rangle$ at 17163 cm^{-1}). At $T = 1.2$ K, one observes a 600 ns emission decay, if the emission of state $|II\rangle$ is detected selectively, for example, on a vibrational satellite ($\bar{\nu}_{det}$:$|II\rangle \rightarrow |0\rangle$ -653 cm^{-1} [44] at 16 510 cm^{-1}). The decay is strictly mono-exponential for more than five lifetimes Fig. 6a. The corresponding decay rate is $k_{exp} = 1/600$ ns $= 1.67 \times 10^6$ s^{-1}. This decay is mainly determined by the direct process of slr from state $|II\rangle$ to state $|I\rangle$. However, similarly as discussed in

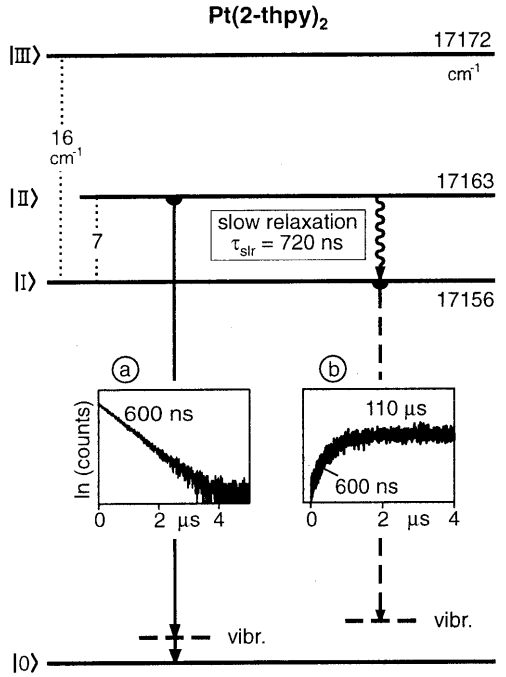

Fig. 6. Triplet sublevels of $Pt(2\text{-thpy})_2$, emission decay and rise behavior in an n-octane matrix (at $T = 1.2$ K) for an excitation energy of $\bar{\nu}_{exc} = 17163$ cm^{-1} (transition $|0\rangle \rightarrow |II\rangle$). The transition at the electronic origin $|0\rangle \leftrightarrow |I\rangle$ is strongly forbidden [44].

Case Study B, the radiative and non-radiative decays from state $|II\rangle$ to the electronic ground state $|0\rangle$ have also to be taken into account according to Eq. (8). With $k_{II} = 2.78 \times 10^5\ s^{-1}$ ($\tau_{II} = 3.6$ μs from Ref. [26]), one obtains k^{slr} ($T = 1.2$ K) $= 1.39 \times 10^6\ s^{-1}$ ($\tau_{slr} = 720$ ns, see Fig. 6).

The relaxation from state $|II\rangle$ to state $|I\rangle$ is also observed in the rise of the emission of state $|I\rangle$, when the excitation energy is kept as before and when the emission is selectively detected on a corresponding vibrational satellite (e.g. $\bar{\nu}_{det}$:$|I\rangle \rightarrow |0\rangle$ $-531\ cm^{-1}$ [44] at 16 625 cm^{-1}). After the rise of this emission intensity, state $|I\rangle$ decays with the usual emission decay time of $\tau_I = 110$ μs. (Compare also the Refs. [16,19,26].)

For completeness, it is mentioned that both states $|I\rangle$ and $|II\rangle$ show significantly different emission spectra, which are super-imposed in time-integrated spectra. Thus, a clear analysis might be difficult. However, by use of the method of time-resolution spectroscopy both spectra can be well separated and more easily assigned. (For details see Ref. [16].) Similar effects are also observed for $[Ru(bpy)_3]^{2+}$ and discussed with regard to further interesting implications in Case Study D (Section 3.4).

3.3.2. Temperature dependence of the spin-lattice relaxation

Fig. 7 shows that the rate of spin-lattice relaxation from state $|II\rangle$ increases distinctly with temperature. The data points are determined from the decay time of

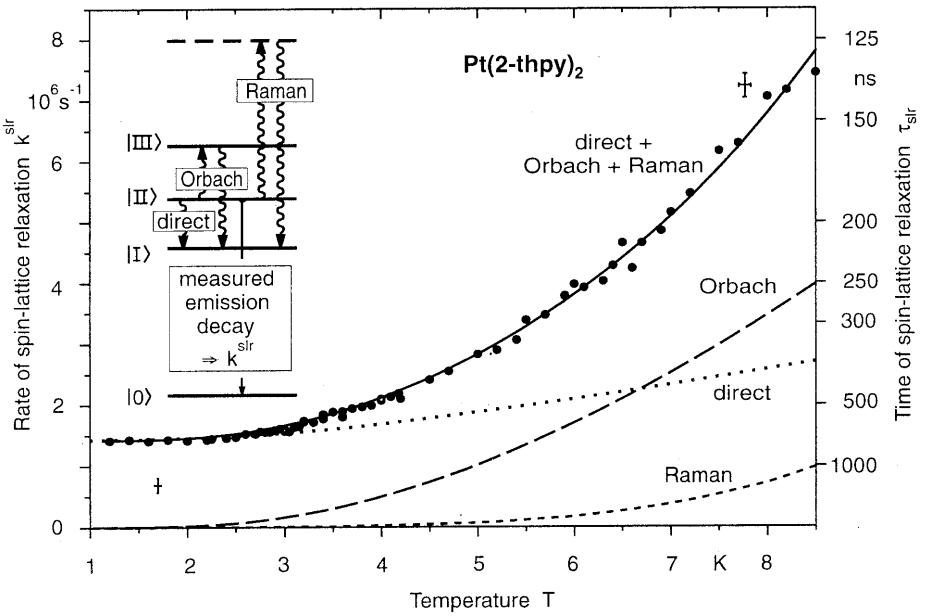

Fig. 7. Temperature dependence of the rate (and time) of spin-lattice relaxation of state $|II\rangle$ of $Pt(2\text{-thpy})_2$ in n-octane. The solid line represents a fit according to Eq. (10) (see text), while the broken and dotted lines give the contributions of the respective processes. (Compare also Ref. [26].) The inset shows the three triplet substates $|I\rangle$, $|II\rangle$, and $|III\rangle$ and sketches the three processes of spin-lattice relaxation.

the emission of state $|II\rangle$ after correcting the corresponding rates, as described above according to Eq. (8). The experimental data can be well fitted, when all three processes of slr, sketched in Fig. 2, are taken into account. In particular, for this specific situation of nearly equally zero-field separated triplet sublevels, one has to apply the extended Orbach expression according to Eq. (2). (In an older investigation [16], we used the original Orbach expression (Eq. (5)), but the fitting procedure led only to an approximate description of the experimental data. In particular, this difficulty triggered our studies [26] to develop the extended Orbach description. Here, we apply an approximation of this more general expression derived in [26].)

Thus, applying the results of Section 2, in particular the Eqs. (1), (2) and (6), and identifying the states $|a\rangle$, $|b\rangle$, and $|c\rangle$ with the triplet sublevels $|I\rangle$, $|II\rangle$, and $|III\rangle$, respectively, one obtains Eq. (10). This equation is used for the fitting procedure to describe the temperature dependence of slr from state $|II\rangle$ to state $|I\rangle$ of Pt(2-thpy)$_2$.

$$k^{slr}(T) = k^{slr}(\text{direct}) + k^{slr}(\text{Orbach}) + k^{slr}(\text{Raman}) \quad (10)$$

This expression contains six parameters after insertion of Eqs. (1), (2) and (6). However, these are reduced to only two free fit parameters, since all energy separations are known from highly resolved spectra (Fig. 6), the ratio $C_{III,I}/C_{III,II}$ is determined to ≈ 1.2 [26,57] from time-resolved excitation spectra, as presented in Ref. [16] and $C_{II,I}$ is equal to the low-temperature limit of the of spin-lattice relaxation rate k^{slr} (direct, $T = 1.2$ K) $= 1/\tau_{slr} = 1.39 \times 10^6$ s^{-1} (see above). Thus the fitting procedure [52] leads to the two unknown parameters and gives the solid line in Fig. 7. (For further details see Ref. [26].)

The results obtained are also used to demonstrate graphically the relative magnitudes of the three different processes that give the total rate of spin-lattice relaxation k^{slr} (T). For the temperature range between 1.2 K $\leq T \leq 3$ K, the total rate k^{slr} is exclusively determined by the direct process. Above $T \approx 3$ K and above ≈ 6 K, the Orbach and the T^5 Raman process, respectively, become important. Although, the Raman process is less significant than the two other processes, its inclusion with $R = (10 \pm 3)$ K^{-5} s^{-1} improves the fit. (R results from the fitting procedure, see Eq. (6).) However, a fit of the data points with a T^7 power law for the Raman process is also possible with slightly different values for the two free fit parameters. But this uncertainly is not unexpected, when one takes into account the contribution of k^{slr} (Raman) with respect to the experimental error (Fig. 7). On the other hand, it has been shown for Pt(2-thpy)(CO)(Cl) that a T^5 dependence is required. Therefore, it seems to be reasonable to adopt this power law also for Pt(2-thpy)$_2$, since both compounds were investigated in the same matrix material (n-octane).

3.3.3. Magnetic field dependence of the spin-lattice relaxation

Pt(2-thpy)$_2$ represents an interesting compound to investigate additionally the influence of high magnetic fields on the rate of spin-lattice relaxation. This is carried out at $T = 1.5$ K [57]. At this temperature, the Raman and the Orbach process do not contribute to the relaxation rate (see Fig. 7). Therefore, the total slr rate is given by the direct process (Eq. (1)). Fig. 8 shows that k^{slr} (direct) increases by a

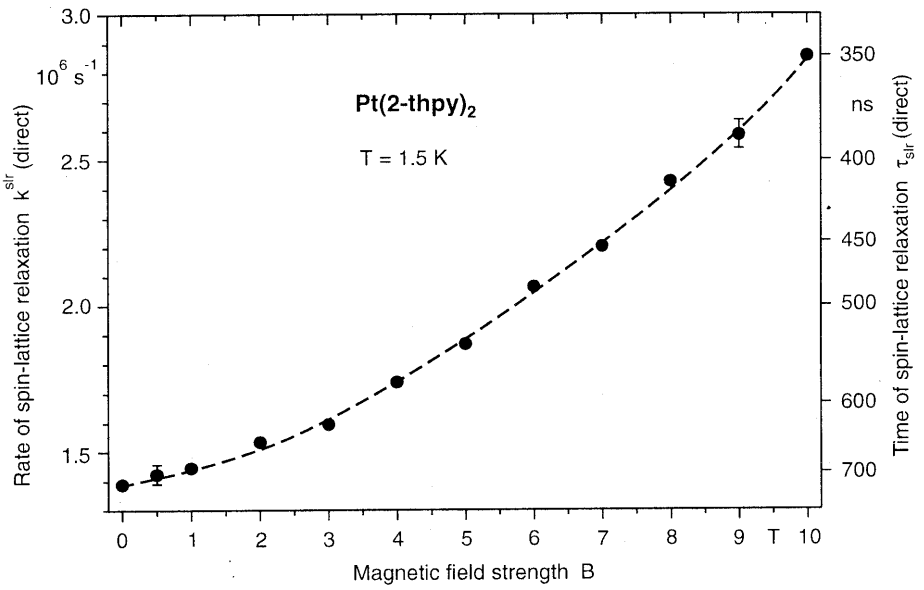

Fig. 8. Magnetic field dependence of the rate (and time) of spin-lattice relaxation of $Pt(2\text{-thpy})_2$ in *n*-octane at $T = 1.5$ K (from Ref. [57]). The data refer to the process of spin-lattice relaxation from state $|II\rangle$ to state $|I\rangle$ and are determined by measuring the emission decay time from state $|II\rangle$. Compare the energy level diagram shown in Fig. 6.

factor of about two under application of a magnetic field of $B = 10$ T. This trend is expected, since the energy difference between the states $|II\rangle$ and $|I\rangle$ increases from $\Delta E_{II,I}$ ($B = 0$ T) $= 7$ cm^{-1} to $\Delta E_{II,I}$ ($B = 10$ T) $= 12$ cm^{-1} [57] due to Zeeman shifts. Thus, the increase of the slr rate seems to be mainly a consequence of the $(\Delta E_{II,I})^3$ dependence (see Eq. (1)).

However, in addition to this cubic dependence on ΔE, one has to consider that the matrix element in Eq. (1) may also be magnetic-field dependent, while the mass density and the velocity of sound are field independent. Fig. 9 illustrates the change of k^{slr} (direct) versus $\{\Delta E_{II,I}(B)\}^3 \cdot \coth\{\Delta E_{II,I}(B)/2k_BT\}$. If the matrix element were constant under application of a B-field, one would expect to find the straight line, which is also plotted in Fig. 9. Obviously, the experimental data show that the matrix element $|\langle II|V|I\rangle|$ becomes smaller with an increasing field. Its value for $B = 0$ T is estimated, similarly as in Case Study B, to ≈ 1.1 cm^{-1} [26], and from Fig. 9 it may be deduced that the matrix element is reduced to ≈ 0.7 cm^{-1} for $B = 10$ T.

The magnetic field induced changes of the matrix element might be related to three different effects:

1. Magnetic fields give rise to mixtures of the three triplet substates. Thus, the matrix element can be altered.
2. An external magnetic field reduces the symmetry of the system, and thus, additional electron phonon couplings can become effective.

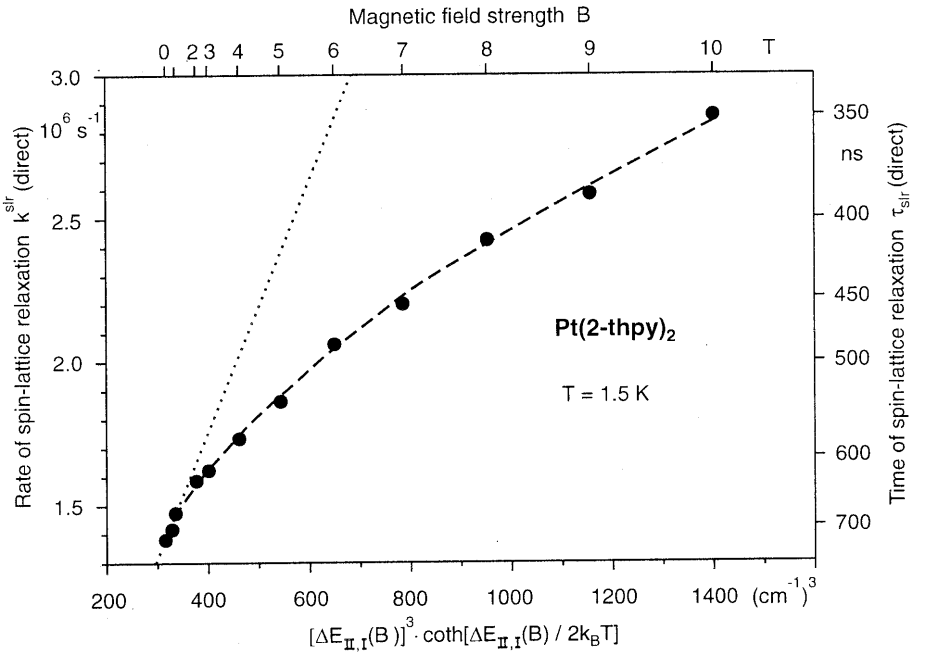

Fig. 9. Rate (and time) of spin-lattice relaxation of Pt(2-thpy)$_2$ in *n*-octane at $T = 1.5$ K for different magnetic fields. The experimental data (points) of Fig. 8 are plotted versus $\{\Delta E_{II,I}(B)\}^3 \cdot \coth\{\Delta E_{II,I}(B)/2k_BT\}$ according to Eq. (1). This expression depends on the external magnetic field B, therefore the corresponding B-scale is given on top of the diagram. (The $\Delta E_{II,I}(B)$ values are taken from Ref. [57].) The plot is shown, to demonstrate the decrease of the squared matrix element $|\langle II|V|I\rangle|^2$ with increasing field. The dotted line characterizes a situation, for which the matrix element is independent from the strength of the magnetic field.

3. A magnetic field, which increases from a low-field limit (Zeeman shift $\ll$ zfs) to the high-field limit (Zeeman shift $\gg$ zfs), induces a change of the orientation of the triplet spins. In the low-field limit the spins are oriented relative to the axes or geometry of the molecule, while in the high-field limit the quantization axis becomes the direction of the external magnetic field (e.g. see Refs. [58]).

Though it is not yet possible to give estimates of these effects with regard to changes of the phonon-induced couplings of the two triplet substrates $|I\rangle$ and $|II\rangle$, we expect that (1) and (2) might lead to a larger matrix element, while according to a very schematic model, the effect (3) should reduce the coupling. In this model (3), it is assumed that at zero field, phonon fluctuations alter both the molecular frame and the orientations of the spins. (Compare Ref. [59].) For high magnetic fields, the spin system is largely oriented with respect to the fixed axis of the external field. Thus, the orientation of the spin system seems to be less effected by phonon fluctuations. This implies that the phonon-induced coupling becomes less efficient with an increasing magnetic field. When the high-field situation is reached, a further significant change of the matrix element or the phonon coupling strength with field increase is not expected in this model (3).

Interestingly, several indications seem to provide a support of model (3): From Fig. 9 it is concluded that for Pt(2-thpy)$_2$ the matrix element is nearly constant for $B < 2$ T (low-field limit) and then decreases with growing field. At $B = 10$ T the separation between the distorted states $|\mathrm{I}\rangle_\mathrm{B}$ and $|\mathrm{II}\rangle_\mathrm{B}$ is about 10 cm^{-1} [57] compared to 7 cm^{-1} at zero field. Obviously, the high-field limit is not yet reached. Indeed, the matrix element still decreases with further field increase.

On the other hand, for Pt(2-thpy)(CO)(Cl) the zfs of the two lowest excited states is only 0.055 cm^{-1} (Case Study B). Therefore, it is expected that the high-field limit is easily reached for field strengths applicable with our equipment. The results show that the Zeeman splitting between these two distorted states $|\mathrm{I}\rangle_\mathrm{B}$ and $|\mathrm{II}\rangle_\mathrm{B}$ can optically be well resolved for $B \geq 2.5$ T. In this situation, it is possible to determine the rate of slr for the process $|\mathrm{II}\rangle_\mathrm{B} \rightarrow |\mathrm{I}\rangle_\mathrm{B}$. Again, the corresponding matrix element decreases however, only up to $B \approx 4$ T. With further field increase it remains constant (at least up to $B = 10$ T), as expected according to model (3). (Results not reproduced here, but see Ref. [57].)

These observations are consistent with the results found for naphthalene, for which the zfs of the lowest triplet is of the order of 0.1 cm^{-1}. For this compound, it has been reported that the slr time follows a strict B^{-3} dependence for high magnetic fields up to $B = 18$ T [60]. Since the Zeeman splitting is proportional to B, this result implies again, as expected from model; (3) that in the high-field limit the matrix element is independent of the magnetic field strength.

In conclusion, the magnetic field dependence of the rate of spin-lattice relaxation is reported here for the first time for metal–organic compounds. These compounds are particularly well suited for such investigations, since the enormous chemical variability allows us to select comparable compounds with suitable sizes of zero-field splittings. Thus, one can study low-, intermediate-, and high-field situations, respectively, in the same range of magnetic field strengths (for example $0 \leq B \leq 12$ T). Such studies open access to interesting information with regard to the dynamics of relaxations within the triplet system of molecules under magnetic fields. Certainly, these first observations and schematic explanations presented here for the magnetic field effects require further investigations.

3.4. Case study D: [Ru(bpy)$_3$]$^{2+}$

[Ru(bpy)$_3$]$^{2+}$ has attracted many research groups due to interesting and unique physical, chemical, biological, and medical properties. A large number of photochemical investigations have been carried out, since electron transfer reactions from the low-lying triplet states can potentially be used for processes to convert solar energy into chemical energy. (For example, see the Refs. [61,62] and [1,2], wherein many references are given.) With regard to the present investigation, [Ru(bpy)$_3$]$^{2+}$ has been chosen, since the lowest triplet is largely of Ru4d-bpy π^* character (^{3}MLCT). Therefore, the metal contribution is essential, as is displayed in the relatively large value of zfs of 61 cm^{-1} of the lowest ^{3}MLCT term (Fig. 1). The metal character has an enormous influence on the excited state properties. In particular, the metal contribution mediates a significant electronic ligand–ligand

coupling, which delocalizes the low-lying electronic states (at least in a rigid matrix) [1,2,6,63]. As further consequence, the compound exhibits only small changes of binding properties upon excitation into these triplets [1,2,4–6]. The importance of the metal character becomes particularly obvious, when spectroscopic properties of $[Ru(bpy)_3]^{2+}$ are compared to those of $[Pt(bpy)_2]^{2+}$ (see case study A in Section 3.1 and Refs. [1,2]) or of $[Rh(bpy)_3]^{3+}$ (see Refs. [1–3]). These latter two complexes exhibit only very small metal participations in the lowest excited states, as is reflected by the values of the total zfs. For example, the value of zfs is by a factor of more than 500 larger for $[Ru(bpy)_3]^{2+}$ (zfs: 61 cm^{-1} [1]) than for $[Rh(bpy)_3]^{3+}$ (zfs: 0.12 cm^{-1} [64,65]). For details with regard to a comparison of photophysical properties see the Refs. [1,2,63].

Fig. 10 shows the energy level diagram for the three lowest triplet substates of $[Ru(bpy)_3]^{2+}$ doped into $[Zn(bpy)_3](ClO_4)_2$. (Compare Refs. [1,2,5,66].) The specific sequence of these states or the zfs pattern leads again to characteristic properties of the dynamics of slr, in particular, for higher temperatures, when the Orbach process becomes important (see below).

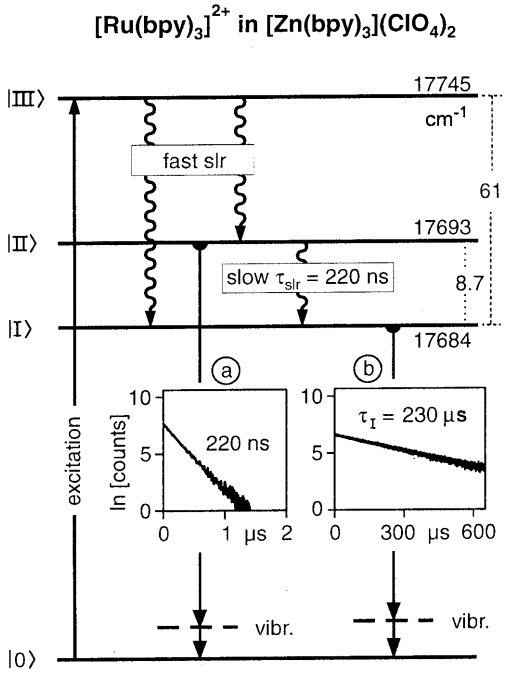

Fig. 10. Low-lying triplet states (^{3}MLCT substates) of $[Ru(bpy)_3]^{2+}$ doped into $[Zn(bpy)_3](ClO_4)_2$. At $T = 1.2$ K, the relaxation from state $|II\rangle$ to state $|I\rangle$ is determined by a direct process of spin-lattice relaxation with $\tau_{slr} = (220 \pm 5)$ ns (a), while the emission from state $|I\rangle$ decays with the usual emission decay time of $\tau_I = (230 \pm 5)$ µs (b). The emission resulting of state $|II\rangle$ cannot be frozen out.

3.4.1. Low-temperature decay properties

After a pulsed excitation, for example into state $|III\rangle$ and at $T = 1.2$ K, the states $|II\rangle$ and $|I\rangle$ are populated by *direct processes* of slr. These are fast, due to the large energy separations of 52 and 61 cm^{-1}, respectively, and due to the $(\Delta E)^3$ dependence of the corresponding rates. (See Eq. (1).) However, according to the comparatively small energy separation of $\Delta E_{II,I} = 8.7$ cm^{-1} between the states $|II\rangle$ and $|I\rangle$, the relaxation time from state $|II\rangle$ to state $|I\rangle$ is again relatively long. Experimentally, this can be seen, when the emission is detected at the electronic origin of the transition $|II\rangle \rightarrow |0\rangle$ (at 17 693 cm^{-1}). At $T = 1.2$ K, one finds an emission decay time of (220 ± 5) ns [1,2,16,19,67,68]. The decay is strictly mono-exponential at least over five decay times Fig. 10(a). The measured value should be corrected similarly as expressed in Eq. (8) by taking into account the radiative and non-radiative decays from state $|II\rangle$ to the electronic ground state $|0\rangle$ with $\tau_{II} = 8$ μs [1] ($k_{II} = 1.3 \times 10^5$ s^{-1}). However, the required correction is less than the experimental error. Thus, the measured decay time can directly be taken as slr time with $\tau_{slr} = 220$ ns ($k^{slr}(\text{direct}) = 4.5 \times 10^6$ s^{-1}).

The usual emission decay time of state $|I\rangle$ of $\tau_I = 230$ μs ($T = 1.2$ K) can be observed as mono-exponential decay, when the emission is detected just on the electronic origin $|I\rangle \rightarrow |0\rangle$ at 17 684 cm^{-1} (Fig. 10b). However, normally, when the condition for this spectral selectivity is not strictly observed, one finds a bi-exponential decay with the two components of 220 ns and 230 μs.

Interestingly, the emissions of the two states $|I\rangle$ and $|II\rangle$ exhibit significant differences with respect to vibronic coupling properties or to the structures of the vibrational satellites [1,2]. Thus, the spectra resulting from the two states differ strongly. Since none of them can be frozen out, even when the temperature is reduced to $T = 1.2$ K, time-integrated spectra represent super-positions of two spectra. This almost general behavior makes an analysis quite difficult. However, it has been shown that the super-imposed spectra can be well separated by measuring time-resolved spectra. Therefore, the spectrum, which is recorded within, for example, the first 300 ns after a short laser pulse (e.g. of ≈ 10 ns), represents nearly exclusively the emission of state $|II\rangle$, while a delayed spectrum (e.g. after $t = 10$ μs) corresponds to the emission of state $|I\rangle$. (For details see Refs. [1,2].)

The effects described above imply that, due to spin-lattice relaxation, the emission spectra shift with time until the population of state $|II\rangle$ is depleted. Taking, for example, five decay times (see Fig. 10a), these shifts will be completed only after ≈ 1 μs. It should be emphasized that such spectral shifts with time have nothing to do with a localization of the excitation on one bpy ligand, as was occasionally assumed.

3.4.2. Temperature dependence and Orbach process

With increasing temperature the slr rate becomes only slightly larger up to $T \approx 6$ K, but with further temperature increase, the rate grows drastically (Fig. 11). This behavior is described by taking into account the direct process (Eq. (1)) and the Orbach process. In the situation of $[Ru(bpy)_3]^{2+}$, for which $\Delta E_{II,I} \ll \Delta E_{III,I}$ and $\Delta E_{III,II}$, one can even use the simple Orbach approximation, given in Eq. (5) by approximating $\Delta E = \Delta E_{III,II} \approx \Delta E_{III,I}$. Thus, the slr rate is described by Eq. (11)

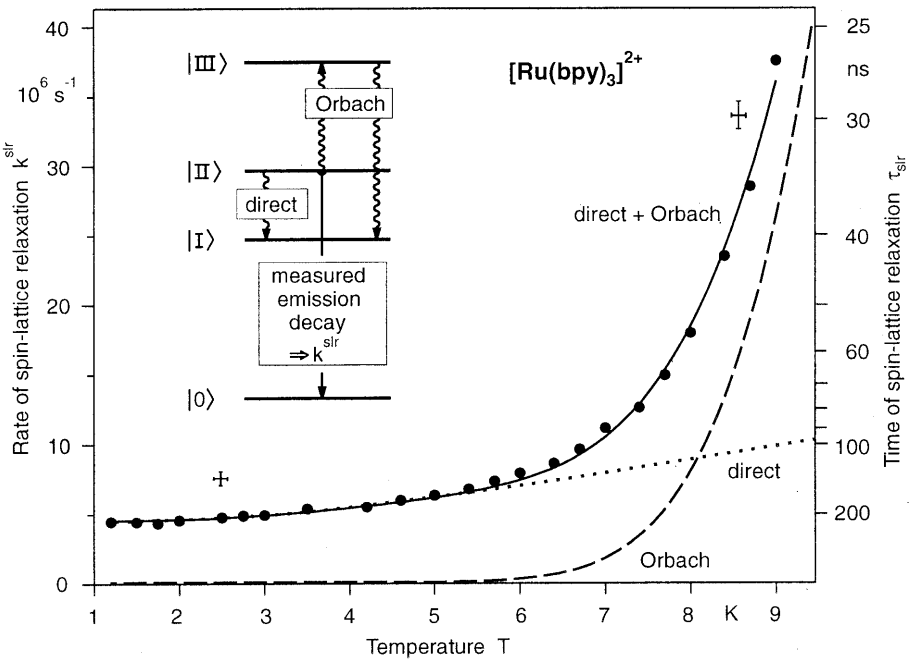

Fig. 11. Temperature dependence of the rate (and time) of spin-lattice relaxation of state $|II\rangle$ of $[Ru(bpy)_3]^{2+}$ doped into $[Zn(bpy)_3](ClO_4)_2$ [1]. The solid line represents a fit according to Eq. (12) (see text), while the broken and the dotted lines give the contributions of the respective processes of spin-lattice relaxation. The inset shows the two processes schematically.

$$k^{slr}(T) = k^{slr}(\text{direct}) + k^{slr}(\text{Orbach}) \tag{11}$$

This expression contains only one free fit parameter (prefactor of Eq. (5)), since the energy separations are known from highly resolved spectra (giving $\Delta E_{II,I} = 8.7$ cm^{-1} and $\Delta E = 52$ cm^{-1}) and since the prefactor of the direct process is determined by the low-temperature value of the slr rate to $k^{slr}(\text{direct}, T = 1.2\ K) = 4.5 \times 10^6\ s^{-1}$. Thus, the experimental data of Fig. 11 can be well fitted by Eq. (12) [1,68].

$$k^{slr}(T)\ [s^{-1}] = 4.5 \times 10^6\ \coth(8.7\ cm^{-1}/2k_BT) + 7.8 \times 10^{10} \cdot \exp(-52\ cm^{-1}/k_BT) \tag{12}$$

For completeness it is mentioned that the consideration of the two processes of slr according to the direct and the Raman process do not fit the experimental data. Also, an inclusion of the Raman process (according to Eq. (6)) as additional, third mechanism does not improve the fit. Obviously, the occurrence of a real electronic state $|III\rangle$ above state $|II\rangle$ by $\Delta E_{III,II} = 52\ cm^{-1}$ strongly favors the Orbach process compared to the Raman process. The relatively large energy separation of 52 cm^{-1} is responsible for the interesting experimental result that the slr rate is only slightly temperature dependent up to $T \approx 6$ K compared to $T \approx 3$ K found for $Pt(2\text{-thpy})_2$ with an energy separation $\Delta E_{III,II} = 9\ cm^{-1}$ (case study C, Section 3.3.2).

3.4.3. Time-resolution and Boltzmann distribution

The discussions presented above have demonstrated that the two lowest excited states of $[Ru(bpy)_3]^{2+}$ are not in a thermal equilibration directly after the laser pulse at low temperature. At $T = 1.2$ K, for example, the relaxation time from state $|II\rangle$ to state $|I\rangle$ is as long as $\tau_{slr} = 220$ ns. It is not expected that at low temperature the populations of these two states are governed by the Boltzmann (Arrhenius) distribution (Compare also the Refs. [31,49,69]). The expected deviation becomes obvious, when ln {Int $II_{ti}(0-0)$/Int$_{ti}I(0-0)$} is plotted versus $1/k_BT$, wherein Int$_{ti}II(0-0)$ and Int $I_{ti}(0-0)$ represent the *time-integrated* (ti) emission intensities at the corresponding electronic origins (see the inset of Fig. 12). The Boltzmann distribution would lead to a straight line (see below), but plot (a) of Fig. 12 demonstrates the non-Boltzmann behavior. The distinct deviation from a straight line is a consequence of the fact that the emission of the higher lying state $|II\rangle$ cannot be frozen out. Thus, the low-temperature ratio measured, for example at $T = 1.2$ K, is determined by the initial populations of the two states and not by thermal equilibration. The same conclusion holds also for the other compounds

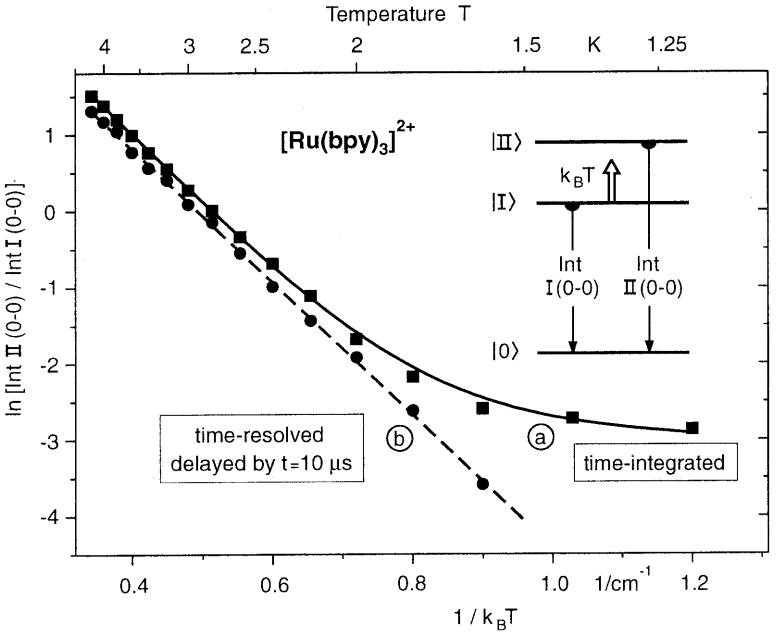

Fig. 12. Boltzmann plots. The diagram shows ratios of emission intensities measured at the electronic origins $|II\rangle \rightarrow |0\rangle$ and $|I\rangle \rightarrow |0\rangle$, respectively, of $[Ru(bpy)_3]^{2+}$ doped into $[Zn(bpy)_3](ClO_4)_2$ (0.3% mol/mol). The data of plot (a) result from time-integrated spectra. This plot demonstrates that the emission of the higher lying state $|II\rangle$ (see inset) cannot be frozen out, due to the effects of spin-lattice relaxation. The curve of plot (a) represents a fit according to Eq. (19) (see text). Data of plot (b) are determined from time-resolved spectra with a time-delay of $t = 10$ µs and a time-window of $\Delta t = 300$ µs. One obtains a strict Boltzmann–Arrhenius behavior with a slope of $\Delta E_{II,I} = (8.7 \pm 0.2)$ cm^{-1} and a ratio of the radiative rates $k^r(|II\rangle \leftrightarrow |0\rangle)/k^r(|I\rangle \leftrightarrow |0\rangle) = (80 \pm 5)$. The same $\Delta E_{II,I}$ value is found in line-narrowed, highly resolved emission spectra [1,2].

discussed in Case Studies A to C. (For details with regard to the emission spectra see the Refs. [1,2,57]).

On the other hand it is expected that the two states $|\mathrm{II}\rangle$ and $|\mathrm{I}\rangle$ will thermally be equilibrated after a certain delay time, for example after $t = 10$ μs. In fact, plot (b) of Fig. 12 demonstrates that the ratio of the corresponding emission intensities at the electronic origins determined from time-resolved and delayed spectra (e.g. see Refs. [1,2,57]) strictly follows the Boltzmann distribution.

$$\frac{\mathrm{Int_d II}(0-0)}{\mathrm{Int_d I}(0-0)} = \frac{k_{\mathrm{II}}^r}{k_{\mathrm{I}}^r} \cdot \exp(-\Delta E_{\mathrm{II,I}}/k_{\mathrm{B}}T) \tag{13}$$

$\mathrm{Int_d II}(0-0)$ and $\mathrm{Int_d I}(0-0)$ are the time-resolved and delayed emission intensities resulting from the states $|\mathrm{II}\rangle$ and $|\mathrm{I}\rangle$, respectively, measured at the electronic origins. k_{II}^r and k_{I}^r are the corresponding radiative decay rates.

The slope of the straight line of plot (b) in Fig. 12 corresponds to the activation energy and is determined to $\Delta E_{\mathrm{II,I}} = (8.7 \pm 0.2)\ \mathrm{cm}^{-1}$. Thus, one obtains a value of the same accuracy as found from highly resolved, line-narrowed emission spectra. (Compare Refs. [1,2]). Moreover, the Boltzmann distribution (plot (b)) provides also the ratio of the radiative rates at the electronic origins of $[\mathrm{Ru(bpy)_3}]^{2+}$ in $[\mathrm{Zn(bpy)_3}](\mathrm{ClO_4})_2$ to $k_{\mathrm{II}}^r/k_{\mathrm{I}}^r = (80 \pm 5)$.

It is highly instructive to demonstrate that the behavior discussed above in a more qualitative way can also be described quantitatively on the basis of rate equations for the two low-lying states $|\mathrm{I}\rangle$ and $|\mathrm{II}\rangle$. An inclusion also of state $|\mathrm{III}\rangle$ into the relaxation kinetics does not seem to be necessary at low temperature, due to its comparatively large energy separations from the two other states (see Fig. 10). It is assumed that the two states $|\mathrm{I}\rangle$ and $|\mathrm{II}\rangle$ are populated by fast slr after an excitation into a higher lying state (e.g. state $|\mathrm{III}\rangle$). The rate equations for the system are given by

$$\frac{\mathrm{d}n_{\mathrm{II}}}{\mathrm{d}t} = -(k_{\mathrm{II}} + k_{\mathrm{II,I}}) \cdot n_{\mathrm{II}} + k_{\mathrm{I,II}} \cdot n_{\mathrm{I}} \tag{14}$$

$$\frac{\mathrm{d}n_{I}}{\mathrm{d}t} = -(k_{\mathrm{I}} + k_{\mathrm{I,II}}) \cdot n_{\mathrm{I}} + k_{\mathrm{II,I}} \cdot n_{\mathrm{II}} \tag{15}$$

wherein n_{II}, n_{I} are the population densities (population per volume) and k_{II}, k_{I} are the total deactivation rates of the states $|\mathrm{II}\rangle$ and $|\mathrm{I}\rangle$ to the ground state $|0\rangle$, respectively. $k_{\mathrm{I,II}}$ and $k_{\mathrm{II,I}}$ represent the upward and downward rates of relaxation between the two triplet sublevels.

With the conditions $k^{\mathrm{slr}} = k_{\mathrm{II,I}} + k_{\mathrm{I,II}} \gg k_{\mathrm{II}}, k_{\mathrm{I}}$ (even at low temperature, compare section 3.4.1) and $k_{\mathrm{I,II}} = k_{\mathrm{II,I}} \mathrm{e}^{-\Delta E/k_{\mathrm{B}}T}$, the population densities of the states $|\mathrm{II}\rangle$ and $|\mathrm{I}\rangle$ can be approximated by the following expressions:

$$n_{\mathrm{II}}(t) \approx \frac{n_{\mathrm{I}}^0 + n_{\mathrm{II}}^0}{1 + \mathrm{e}^{\Delta E/k_{\mathrm{B}}T}} \cdot \mathrm{e}^{-(k^{\mathrm{therm}}\, t)} + \frac{n_{\mathrm{II}}^0 - n_{\mathrm{I}}^0 \mathrm{e}^{-\Delta E/k_{\mathrm{B}}T}}{1 + \mathrm{e}^{-\Delta E/k_{\mathrm{B}}T}} \cdot \mathrm{e}^{-k^{\mathrm{slr}} t} \tag{16}$$

$$n_{\mathrm{I}}(t) \approx \frac{n_{\mathrm{I}}^0 + n_{\mathrm{II}}^0}{1 + \mathrm{e}^{-\Delta E/k_{\mathrm{B}}T}} \cdot \mathrm{e}^{-(k^{\mathrm{therm}} t)} - \frac{n_{\mathrm{II}}^0 - n_{\mathrm{I}}^0 \mathrm{e}^{-\Delta E/k_{\mathrm{B}}T}}{1 + \mathrm{e}^{-\Delta E/k_{\mathrm{B}}T}} \cdot \mathrm{e}^{-k^{\mathrm{slr}} t} \tag{17}$$

with $\Delta E = \Delta E_{\mathrm{II,I}}$ and n_{I}^0, $n_{\mathrm{II}}^0$the population densities at $t = 0$s.$k^{therm} = 1/\tau^{\mathrm{therm}} = k_{\mathrm{I}} + k_{\mathrm{II}}\mathrm{e}^{-\Delta E/k_{\mathrm{B}}T}$ is the inverse decay time of the system of two thermalized triplet substates.

The emission intensity Int(t) of a transition at time t is directly proportional to the radiative rate k^r and the population density $n(t)$ of the corresponding state. Therefore, the emission intensity for a given time-window Δt, as measured by time-resolved spectra, can be obtained by multiplication of Eq. (16) and Eq. (17), respectively, with the corresponding radiative rates and subsequent integration over Δt.

In the situation of a delayed detection with a long delay time of, for example $t = 10$ μs, the second terms in the Eqs. (16) and (17) can be neglected, since the slr time $\tau_{\mathrm{slr}} = 1/k^{\mathrm{slr}}$ is several orders of magnitude shorter than the decay time of the emission to the ground state. Thus, one obtains for the intensity ratio measured after a sufficiently long time delay

$$\frac{\mathrm{Int}_d\mathrm{II}(0-0)}{\mathrm{Int}_d\mathrm{I}(0-0)} = \frac{k_{\mathrm{II}}^r \int_{10\mu s}^{\infty} n_{\mathrm{II}}(t)\,\mathrm{d}t}{k_{\mathrm{I}}^r \int_{10\mu s}^{\infty} n_{\mathrm{I}}(t)\,\mathrm{d}t} \approx \frac{k_{\mathrm{II}}^r}{k_{\mathrm{I}}^r} \cdot \exp(-\Delta E/k_{\mathrm{B}}T) \tag{18}$$

This result represents the Boltzmann distribution as already presented in Eq. (13) with $\Delta E = \Delta E_{\mathrm{II,I}}$. Exactly, this behavior is observed experimentally. (Plot (b)) in Fig. 12).

If, on the other hand, the emission is detected for the complete decay time after a short excitation pulse, as measured by time-integrated (ti) spectra, both terms of Eqs. (16) and (17), respectively, have to be taken into account. Neglecting the rise in the emission of state $|\mathrm{I}\rangle$, one obtains for the ratio of the emission intensities of the substates $|\mathrm{II}\rangle$ and $|\mathrm{I}\rangle$ at the electronic origins

$$\frac{\mathrm{Int}_{\mathrm{ti}}\mathrm{II}(0-0)}{\mathrm{Int}_{\mathrm{ti}}\mathrm{I}(0-0)} = \frac{k_{\mathrm{II}}^r \int_0^{\infty} n_{\mathrm{II}}(t)\,\mathrm{d}t}{k_{\mathrm{I}}^r \int_0^{\infty} n_{\mathrm{I}}(t)\,\mathrm{d}t} \approx$$

$$\frac{k_{\mathrm{II}}^r}{k_{\mathrm{I}}^r}\left\{\exp[-\Delta E/k_{\mathrm{B}}T] + \frac{\left(\frac{n_{\mathrm{II}}^0}{n_{\mathrm{I}}^0} - \exp[-\Delta E/k_{\mathrm{B}}T]\right)(k_{\mathrm{I}} + k_{\mathrm{II}}\exp[-\Delta E/k_{\mathrm{B}}T])}{\left(\frac{n_{\mathrm{II}}^0}{n_{\mathrm{I}}^0} + 1\right)k^{\mathrm{slr}}(T)}\right\} \tag{19}$$

$k^{\mathrm{slr}}(T)$ describes the temperature dependence of the slr rate. As expected, fast slr between the triplet sublevels ($\tau_{\mathrm{slr}} \to 0$ s *or* $k^{\mathrm{slr}} \to \infty$) leads to a vanishing second term of Eq. (19), and one obtains the Boltzmann distribution as in Eqs. (13) and (18).

In particular, when the slr rate is small, the second term of Eq. (19) leads to the deviation from the Boltzmann distribution, as is found in plot (a) of Fig. 12. With raising temperature $k^{\mathrm{slr}}(T)$ increases (see Fig. 11 and Eq. (12)). Thus, the second term of Eq. (19) becomes less important. This is also displayed by plot (a) of Fig.

12. In summary, the experimental data of the time-integrated measurements can be fitted by Eq. (19) with only one free fit parameter. $\Delta E = \Delta E_{II,I} = 8.7\ cm^{-1}$ is known from highly resolved spectra and $k_{II}^r/k_I^r = 80$ results from plot (b) of Fig. 12. k_I and k_{II} result from the emission decay times for the corresponding transitions to the electronic ground state with $k_I = 1/\tau_I = 1/230$ μs and $k_{II} = 1/\tau_{II} = 1/8$ μs. (See Section 3.4.1 and Ref. [1].) Further, $k^{slr}(T)$ is displayed in Fig. 11 and given by Eq. (12). Thus, the one free fit parameter n_{II}^0/n_I^0 is obtained by the fitting procedure to (0.6 ± 0.2). This value characterizes the ratio of the initial populations of the two states $|II\rangle$ and $|I\rangle$ after a pulsed excitation into state $|III\rangle$. Interestingly, the same value has been determined independently from time-resolved excitation measurements [16,57].

3.4.4. Pressure dependence of spin-lattice relaxation

The slr rate of a doped molecule depends on the properties of the matrix material (e.g. see Eq. (1)) and how the matrix cage couples to the electronic states of the chromophore. These latter interactions are only rarely discussed in detail and therefore are not completely taken into account by the theoretical models discussed in Section 2. It has been shown recently [26] that different sites of $Pt(phpy)_2$ (with phpy = 2,2′-phenylpyridinate) in the same n-octane matrix exhibit slr rates, which differ by about a factor of three, when rates according to the direct process of slr are compared. These investigations [26] indicate further that those chromophore sites, which are more strongly perturbed by the matrix cage, exhibit the larger slr rates. In this context, it is of interest to expose the chromophore-cage system to a physically better defined external perturbation, as is given by application of high pressure.

Fig. 13 shows the dependence of the slr rate on applied high pressure up to $p = 20$ kbar, at $T = 2$ K. To our knowledge, similar investigations have not yet been reported in the literature. For $[Ru(bpy)_3]^{2+}$, the time of slr $\tau_{slr} = 1/k^{slr}$ is given by the fast decaying emission component of state $|II\rangle$ (compare Fig. 10). At $T = 2$ K, the Orbach process is frozen out (Fig. 11). Thus, the rate shown in Fig. 13 reflects the slr according to the direct process. The rate increases (at $T = 2$ K) from k^{slr} (direct, $p = 0$ kbar) $= 4.5 \times 10^6\ s^{-1}$ to k^{slr} (direct, $p = 20$ kbar) $\approx 20 \times 10^6\ s^{-1}$, i.e. by more than a factor of four (details of the experimental equipment are found, for example, in Refs. [46,70–72]).

Obviously, high pressure compresses the matrix cage and thus gives rise to an increase of the chromophore-cage interaction. This can have two consequences: (i) The wavefunctions of the two states $|I\rangle$ and $|II\rangle$ become more strongly mixed, which would lead to an increase of $\Delta E_{II,I}$ by high pressure application. Thus, also the slr rate should grow due to the $(\Delta E_{II,I})^3$ dependence of k^{slr} (direct) (compare Eq. (1)). However, in independent investigations [71,73], it was possible, to determine the pressure-induced shifts of both electronic origins I ($|0\rangle \leftrightarrow |I\rangle$) and II ($|0\rangle \leftrightarrow |II\rangle$) also at low temperature ($T \approx 2$ K) to be $\Delta\bar{\nu}/\Delta p = -(12.7 \pm 1)\ cm^{-1}\ kbar^{-1}$. Within limits of experimental error, $\Delta E_{II,I}$ does not change in the applied pressure

range up to ≈ 16 kbar. Therefore, a second (ii) effect seems to be more important. The compression of the chromophore-matrix cage strengthens also the electron-phonon coupling. This leads to an increase of the matrix element (see Eq. (1)) with pressure application. However, the prefactors of Eq. (1) have also to be considered. The mass density ρ and the velocity of sound v in the fifth power appear in the denominator. Since both values usually increase with application of pressure (e.g. compare Refs. [74,75]), the slr rate should even decrease under assumption of an unchanged matrix element. Thus, although data for $\rho(p)$ and $v(p)$ are not available, it can be concluded that the increase of the (squared) matrix element is even much more pronounced than displayed by the increase of k^{slr} in Fig. 13.

Interestingly, application of high pressure and of high magnetic fields, respectively, induce a pronounced increase of the rate of spin-lattice relaxation according to the direct process. However, both effects are caused by different physical or quantum mechanical mechanisms. For the compounds discussed, high pressure alters mainly the interaction of the chromophore with its matrix environment, while application of a magnetic field results in an increase of energy separations by Zeeman shifts and additionally leads to a change of the orientation of the spin system. These schematic models require certainly further investigations.

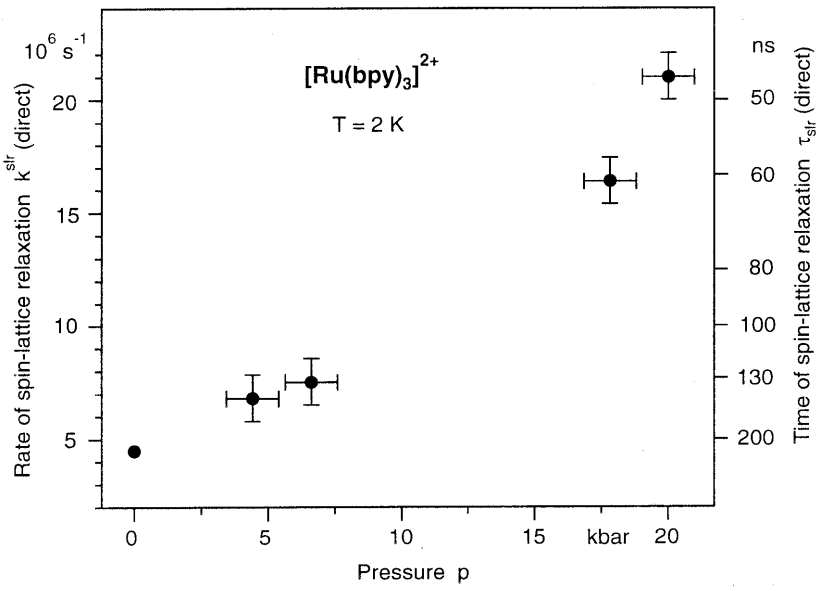

Fig. 13. Pressure dependence of the rate (and time) of spin-lattice relaxation of state $|II\rangle$ to state $|I\rangle$ in $[Ru(bpy)_3]^{2+}$ doped into $[Zn(bpy)_3](ClO_4)_2$ (0.3% mol/mol) ($T = 2$ K, detection at the electronic origin $|II\rangle \rightarrow |0\rangle$). The experimental data are normalized, in order to obtain at $p = 0$ kbar the same value of $k^{slr}(\text{direct}) = 4.5 \times 10^6$ s^{-1} inside and outside the high pressure cell.

4. Conclusions

In metal–organic complexes, the lowest excited electronic state is very often a triplet, while the ground state is a singlet. The properties of this triplet are strongly determined by spin-orbit coupling induced by the metal. In particular, when the metal belongs to the platinum metal group, the effective spin-orbit coupling can be relatively large. This leads to a significantly different emission behavior than that of organic emitters. For example, the intersystem crossing from the lowest singlet S_1 to the lowest triplet T_1 is mostly so fast that no S_1 fluorescence occurs. The compounds exhibit only phosphorescence from T_1. Moreover, T_1 is often zero-field split by several wavenumbers into three substates, and these can even be excited directly from the electronic ground state S_0. Important is that every substate can carry individual photophysical or photochemical properties, like different initial populations after excitation into a higher lying singlet, different radiative and non-radiative rates of transitions to the ground state, etc. Moreover, after initial populations of the individual sublevels, one observes very specific and in part astonishingly slow changes of the populations, in particular at low temperature. The dynamical phenomena are described by spin-lattice relaxations (slr). These do not only depend on the individual wavefunctions of the substates, but essentially on the splitting patterns of the triplet term, on temperature, on properties of the matrix material, and how the matrix interacts with the substates. Corresponding theoretical models are well known, namely the direct process, the Orbach process, and the Raman process (e.g. see Ref. [10] and Fig. 2).

In the present study, it is demonstrated that metal–organic or related compounds of the platinum metal group are particularly well suited to investigate these important processes of spin-lattice relaxation, due to the possibility of tuning properties and zfs patterns of the triplet system by chemical variation. This is mainly a consequence of the tunability of the metal-d or MLCT participation in the wavefunctions of the low-lying triplet substates. In Table 1 we summarize a number of compounds to demonstrate the wide variability of properties and the almost general importance of effects of spin-lattice relaxation. It is not in the scope of this review to discuss all individual compounds comprehensively. The data given in Table 1 - *being largely arranged according to an increasing zero-field splitting of* $\Delta E_{II,I}$ - may be used as an outlook to stimulate further, more detailed studies. In this review four different compounds, included in Table 1, namely $[Pt(bpy)_2]^{2+}$, Pt(2-thpy)(CO)(Cl), $Pt(2\text{-thpy})_2$, and $[Ru(bpy)_3]^{2+}$, with total zfs ranging from the order of 0.1 to 61 cm^{-1} (Fig. 1) are discussed as representative case studies. By these investigations, one obtains a deeper and more general understanding of the population dynamics occurring in triplet systems. Some of the trends observed are summarized:

- The relaxation time from a higher lying sublevel to a lower lying one can be as long as many nano-seconds to several micro-seconds and formally even longer than the decay time to the electronic ground state, at $T = 1.2$ K. During this time, a thermal equilibration or a Boltzmann distribution is not given. This is even valid for levels, that are split only by 0.1–0.2 cm^{-1} at $T = 1.3$ K ($k_B T = 0.9$

cm^{-1}) as in $[Pt(bpy)_2]^{2+}$. Also populations of states that lie several cm^{-1} higher than the lowest excited state can mostly not be frozen out. In these situations the different sublevels decay with different time constants, show super-imposed emission or excited state absorption spectra, and can exhibit different properties of energy transfer (e.g. see Refs. [21–23]). For clear assignments, it is important that the corresponding investigations are carried out with spectroscopic methods, which exhibit a selectivity with regard to the respective states, like methods of time-resolution (e.g. see Refs. [1,2,16–20]) or like double resonance methods (e.g. ODMR spectroscopy) for smaller energy separations (e.g. see Refs. [30–40,64,65]).

- The rates of spin-lattice relaxation increase with temperature and the thermal equilibration between the states becomes much faster. It is shown that the temperature dependence, observed for the different compounds, can quantitatively be described by taking into account the direct, the Orbach and/or the Raman process.
- The spin-lattice relaxation between two energy levels split by several cm^{-1} occurs in a low-temperature range only according to a direct process. This process shows a very slight temperature dependence. The temperature, at which an additional process becomes important is essentially determined by the occurrence of a third electronic state and its energy separation from the other two states. The third state can, for example, be the third triplet substate. For $Pt(2\text{-thpy})_2$ and $[Ru(bpy)_3]^{2+}$, one finds a medium and a large energy separation, respectively, and thus the temperature range, which is governed only by the direct process goes up to $T \approx 3$ K and ≈ 6 K, respectively. Above these temperatures, the Orbach process, that depends exponentially on T, grows in. If no real electronic state is present, like in Pt(2-thpy)(CO)(Cl) (above state $|III\rangle$), the Orbach process is unimportant. In this situation the Raman process according to a T^5 power law becomes dominant at higher temperatures.
- For a number of metal–organic compounds the three triplet sublevels are nearly symmetrically split, as is found for $Pt(2\text{-thpy})_2$. In this situation, the original Orbach expression cannot be used. But an extended expression [26,27] developed only recently for these types of patterns of zero-field splitting can be applied successfully to describe the temperature dependence of the rate of spin-lattice relaxation.
- Application of an external high pressure causes a strong increase of the rate of spin-lattice relaxation at $T = 2$ K, as is shown for $[Ru(bpy)_3]^{2+}$ doped into $[Zn(bpy)_3](CO_4)_2$. At this temperature only the direct process is effective. Pressure application up to 20 kbar results in an increase of k^{slr} (direct) by a factor of more than four. This behavior is ascribed to a compression of the matrix cage surrounding the chromophore. It results in a larger coupling of the matrix to the electronic states involved. This explanation compares well to the results found for different sites (different cage structures) of $Pt(phpy)_2$ in *n*-octane at ambient pressure [26]. For this latter compound, it has been shown that the rates of spin-lattice relaxation differ significantly for the different cage structures.

Table 1
Energies of electronic states (cm^{-1}), emission decay and spin-lattice relaxation times of triplet sublevels ($|I\rangle$, $|II\rangle$, $|III\rangle$) at $T \leq 1.3$ K

Compound	Lowest electronic origin I	Energy separations to state $\|I\rangle$		Emission decay times (μs)			slr time (ns)	Assignments [d]	Remarks references
		$\Delta E_{II,I}$	$\Delta E_{III,I}$	τ_I	τ_{II}	τ_{III}	τ_{slr}		
$[Rh(bpy)_3]^{3+}$ [a]	22 757	0.04 cm^{-1} (1.18GHz) [b] 0.077 cm^{-1} (2.32GHz) [b] 0.116 cm^{-1} (3.49GHz) [b]		4.5×10^3	1.35×10^3	0.65×10^3	$\gg \tau_I$ 10^9 [c]	^{3}LC + small dd* admixtures	[1–3,40,64,65]
$Pd(qol)_2$ [e,f]	16 090	0.0785 cm^{-1} (2.356 GHz) [b] 0.175 cm^{-1} (5.241 GHz) [b]		90×10^3	180	80	$\gg \tau_I$	^{3}ILCT	Site of lowest energy [30,40,43]
$Pd(2\text{-thpy})_2$ [e,f]	18 418	0.0962 cm^{-1} (2.886 GHz) [b]		1.2×10^3	235	130	$\gg \tau_I$	^{3}LC + MLCT admixtures	[17,39,40,43,56,76]
$[Pt(bpy)_2]^{2+}$ [e,g]	21 237	0.2 [c]	0.2 [c]	50	8	3	$\gg \tau_I$	^{3}LC + small MLCT admixtures	**Case Study A.** Investigation at $T = 1.3$ K; [1,2,20,41]
$Pt(qol)_2$ [e,f]	15 426	<1	<1	60	13	4.5	[i]	^{3}ILCT	[18,42,43]
Pt(qtl) [f,h]	13 158	<1	<1	7	2.8	0.55	[i]	^{3}ILCT	[42,43]
Pt(2-thpy)-(CO)(Cl) [e,f]	18 012.5	0.055 [b]	3.8	120	45	35	3.0×10^3 [j]	^{3}LC + MLCT admixtures	**Case Study B.** Investigation: $\tau_{slr}(T)$ [19,43,47,57]
Pt(phpy)-(CO)(Cl) [f,k]	20 916.0	≈ 0.1 [c]	6.4	[i]	[i]	[i]	[i]	^{3}LC + MLCT admixtures	[19,43]
$Pt(phpy)_2$ [e,f]	19 571	6.9	32	70	2.4	[i]	390	^{3}LC/MLCT	Site of lowest energy [19,26,57,77]
$Pt(2\text{-thpy})_2$ [e,f]	17 156	7	16	110	3.6	[i]	720	^{3}LC + MLCT admixtures	**Case Study C.** Investigations: $\tau_{slr}(T)$; $\tau_{slr}(B)$ [4,6,16,19,25,43,44, 56,57,76,77]

Table 1 (*Continued*)

Compound	Lowest electronic origin I	Energy separations to state $\|I\rangle$		Emission decay times (μs)			slr time (ns)	Assignments [d]	Remarks references
		$\Delta E_{II,I}$	$\Delta E_{III,I}$	τ_I	τ_{II}	τ_{III}	τ_{slr}		
$[Ru(bpdz)_3]^{2+}$ [a,l]	17 346	8	61	195	[i]	[i]	410	^{3}MLCT	[1,19,41]
$[Ru(bpz)_3]^{2+}$ [a,m]	18 226	8.5	54	400	[i]	[i]	180	^{3}MLCT	[1,19,41]
$[Ru(bpy)_3]^{2+}$ [a,e]	17 684	8.7	61	230	8	0.9	220	^{3}MLCT	**Case Study D.** Investigations: $\tau_{slr}(T)$; $\tau_{slr}(p)$ [1–6,16,63, 67,71,73]
$Pt(bhq)_2$ [e,n]	19 814	11	38	[i]	[i]	[i]	[i]	^{3}LC/MLCT	[78]
$Pt(3\text{-}thpy)_2$ [e,f]	18 020	13	22	105	2.7	5	≈25	^{3}LC + MLCT admixtures	[77,79]
$[Os(bpy)_3]^{2+}$ [a,e]	14 223	63	221	22	[i]	[i]	[i]	^{3}MLCT	[1,4,80]

[a] In $[Zn(bpy)_3](ClO_4)_2$.
[b] ODMR transition.
[c] Estimated order of magnitude.
[d] LC: ligand centered; MLCT: metal-to-ligand charge transfer; ILCT: intra-ligand charge transfer.
[e] Compare structure formulae in Fig. 1.
[f] In *n*-octane.
[g] Trap in neat $[Pt(bpy)_2](ClO_4)_2$.
[h] $(qtl)^-$ = 8-quinolinethiolate.
[i] Not yet determined.
[j] The spin-lattice relaxation time τ_{slr} is given for the process from state $|III\rangle$ to the states $|I\rangle$ and $|II\rangle$. In all other cases τ_{slr} refers to the process from state $|II\rangle$ to state $|I\rangle$.
[k] $(phpy)^-$ = phenylpyridinate.
[l] (bpdz) = 3,3′-bipyridazine.
[m] (bpz) = 2,2′-bipyrazine
[n] In *n*-decane.

- Application of magnetic fields up to $B = 10$ T on $Pt(2\text{-thpy})_2$ in *n*-octane (at $T = 1.5$ K) leads to an increase of k^{slr} (direct) by a factor of two. However, based on the size of the *B*-field induced increase of the energy separation between the perturbed triplet substates, one would expect to find a much larger effect on the rate of spin-lattice relaxation. In a very schematic model, this behavior is explained on the basis of a transition from a low-field to an intermediate-field case, whereby the quantization axis of the spin system changes. With increasing magnetic field the spins become less coupled to the molecular frame but become oriented relative to the direction of the external magnetic field. It is proposed that in this latter situation the phonons interact less efficiently with the triplet substates. Thus, by application of magnetic fields, the matrix element, which couples the triplet substates to the phonons becomes smaller. Obviously, magnetic fields influence the spin-lattice relaxation by a totally different physical mechanism than high pressure, although both external distortions cause an increase of the corresponding rate.

Acknowledgements

We thank Dr Werner Humbs for the preparation of $Pt(2\text{-thpy})_2$ and for measuring the emission decay data of $[Pt(bpy)_2]^{2+}$ (PhD-Thesis). Professor K.P. Balashev and his group is acknowledged for the preparation of Pt(2-thpy)(CO)(Cl). We also thank the Degussa AG (Hanau, Germany) for donation of $K_2[PtCl_4]$ and $RuCl_3 \cdot 3H_2O$. This investigation was financially supported by the Fonds der Chemischen Industrie and the Deutsche Forschungsgemeinschaft.

References

[1] H. Yersin, W. Humbs, J. Strasser, Electronic and Vibronic Spectra of Transition Metal Complexes, in: H. Yersin (Ed.), Topics in Current Chemistry 191, vol. II, Springer, Germany, 1997, p. 153.
[2] H. Yersin, W. Humbs, J. Strasser, J. Coord. Chem. Rev. 159 (1997) 325.
[3] W. Humbs, H. Yersin, Inorg. Chem. 35 (1996) 2220.
[4] H. Yersin, P. Huber, H. Wiedenhofer, Coord. Chem. Rev. 132 (1994) 35.
[5] H. Yersin, D. Braun, Chem. Phys. Lett. 179 (1991) 85.
[6] H. Yersin, W. Humbs, Inorg. Chem. 38 (1999) 5820.
[7] I. Waller, Z.f. Physik 79 (1932) 370.
[8] R.L. de Kronig, Physica 6 (1939) 33.
[9] J.H. van Vleck, Phys. Rev. 57 (1940) 426.
[10] P.L. Scott, C.D. Jeffries, Phys. Rev. 127 (1962) 32.
[11] R. Orbach, M. Blume, Phys. Rev. Lett. 8 (1962) 478.
[12] A.A. Manenkov, R. Orbach, Spin-Lattice-Relaxation in Ionic Solids, Harper & Row, New York, 1966.
[13] M.B. Walker, Can. J. Phys. 46 (1968) 1347.
[14] A. Abragam, B. Bleaney, Electron Paramagnetic Resonance of Transition Ions, Clarendon Press, Oxford, 1970.
[15] B. Henderson, G.F. Imbusch, Optical Spectroscopy of Inorganic Solids, Clarendon Press, Oxford, 1989.

[16] J. Schmidt, J. Strasser, H. Yersin, Inorg. Chem. 36 (1997) 3957.
[17] J. Schmidt, H. Wiedenhofer, A. von Zelewsky, H. Yersin, J. Phys. Chem. 99 (1995) 226.
[18] D. Donges, J.K. Nagle, H. Yersin, Inorg. Chem. 36 (1997) 3040.
[19] J. Strasser, D. Donges, W. Humbs, M.V. Kulikova, K.P. Balashev, H. Yersin, J. Luminescence 76–77 (1998) 611.
[20] W. Humbs, H. Yersin, Inorg. Chim. Acta 265 (1997) 139.
[21] H. Yersin, G. Hensler, E. Gallhuber, J. Luminescence 40–41 (1988) 676.
[22] D. Braun, H. Yersin, Inorg. Chem. 34 (1995) 1967.
[23] H. Yersin, D. Braun, E. Gallhuber, G. Hensler, Ber. Bunsenges. Phys. Chem. 91 (1987) 1228.
[24] V.A. Andreev, Y.I. Prilutskii, Phys. Solid State 35 (1993) 1624.
[25] V.A. Andreev, Y.I. Prilustkii, Sov. Phys. Solid State (engl. translation) 34 (1992) 1178.
[26] J. Strasser, H.H.H. Homeier, H. Yersin, Chem. Phys., in press.
[27] H.H.H. Homeier, J. Strasser, H. Yersin, Chem. Phys. Lett. 316 (2000) 280.
[28] R. Orbach, M. Blume, Phys. Rev. Lett. 8 (1962) 478.
[29] L.H. Hall, M.A. El-Sayed, Chem. Phys. 8 (1975) 272.
[30] H. Yersin, D. Donges, J.K. Nagle, R. Sitters, M. Glasbeek, Inorg. Chem. 39 (2000) 770.
[31] D.S. Tinti, M. El-Sayed, J. Chem. Phys. 54 (1971) 2529.
[32] S. Yamauchi, T. Azumi, Chem. Phys. Lett. 21 (1973) 603.
[33] D.S. Tinti, M.A. El-Sayed, A.H. Maki, C.B. Harris, Chem. Phys. Lett. 3 (1969) 343.
[34] D. Schweitzer, K.H. Hausser, H. Vogler, F. Diederich, H.A. Staab, Mol. Phys. 46 (1982) 1141.
[35] N. Okabe, T. Ikeyama, T. Azumi, Chem. Phys. Lett. 165 (1990) 24.
[36] A.L. Kamyshny, A.P. Suisalu, L.A. Aslanov, Coord. Chem. Rev. 117 (1992) 1.
[37] Y. Komoda, S. Yamamauchi, N. Hirota, J. Phys. Chem. 90 (1986) 6425.
[38] T. Azumi, H. Miki, Electronic and Vibronic Spectra of Transition Metal Complexes, in: H. Yersin (Ed.), Topics in Current Chemistry 191, vol. II, Springer, Germany, 1997, p. 1.
[39] M. Glasbeek, R. Sitters, E. van Veldhoven, A. von Zelewesky, W. Humbs, H. Yersin, Inorg. Chem. 37 (1998) 5159.
[40] M. Glasbeek, Transition Metal and Rare Earth Compounds - Excited States, Transitions, Interactions, in: H. Yersin (Ed.), Topics in Current Chemistry, Springer, Germany, (2000) in press
[41] W. Humbs, PhD-Thesis, Universität Regensburg 1997.
[42] D. Donges, J.K. Nagle, H. Yersin, J. Luminescence 72–74 (1997) 658.
[43] D. Donges, PhD-Thesis, Universität Regensburg 1997.
[44] H. Wiedenhofer, S. Schützenmeier, A. von Zelewsky, H. Yersin, J. Phys. Chem. 99 (1995) 13385.
[45] E.V. Shpol'skii, Sov. Phys. Usp. (Eng. Transl.) 3 (1960) 372.
[46] H. Yersin, D. Trümbach, H. Wiedenhofer, Inorg. Chem. 38 (1999) 1411.
[47] W. Humbs, M. Glasbeek, R. Sitters, H. Yersin, submitted.
[48] R.W. Harrigan, G.A. Crosby, J. Chem. Phys. 59 (1973) 3468.
[49] T. Azumi, C.M. O'Donnell, S.P. McGlynn, J. Chem. Phys. 45 (1966) 2735.
[50] N. Normann, H. Mathisen, Acta Chem. Scand. 26 (1972) 3913.
[51] J.R. Green, C.E. Scheie, J. Phys. Chem. Solids 28 (1967) 383.
[52] Fit program of Microcal™ Origin; Version 4,10, 32 Bit; Microcal Software Northhampton, MA, USA.
[53] V. Balzani, M. Maestri, A. Melandri, D. Sandrini, L. Chassot, C. Cornioley-Deuschel, P. Jolliet, U. Maeder, A. von Zelewsky, in: H. Yersin, A. Vogler (Eds.), Photochemistry and Photophysics of Coordination Compounds, Springer, Germany, 1987, p. 71.
[54] L. Chassot, A. von Zelewsky, Inorg. Chem. 26 (1987) 2814.
[55] M. Maestri, V. Balzani, C. Deuschel-Cornioley, A. von Zelewsky, Adv. Photochem. 17 (1992) 1.
[56] K. Pierloot, A. Ceulemans, M. Merchán, L. Serrano-Andrés, J. Phys. Chem., submitted.
[57] J. Strasser, PhD-Thesis, Universität Regensburg 1999.
[58] (a) U. Konzelmann, D. Kilpper, M. Schwoerer, Z. Naturforsch. Teil a 30 (1975) 754. (b) N.J. Turro, Modern Molecular Photochemistry, The Benjamin/Cummings Publ. Menlo Park, California 1978, p. 27. (c) G.W. Canters, J.H. van der Waals in: D. Dolphin (Ed.), The Porphyrins, vol. III, Acad. Press, New York 1978, p. 560.

[59] P.J.F. Verbeek, A.I.M. Dicker, J. Schmidt, Chem. Phys. Lett. 56 (1978) 585.
[60] K.F. Renk, H. Sixl, H. Wolfrum, Chem. Phys. Lett. 52 (1977) 98.
[61] A. Juris, V. Balzani, F. Barigelletti, S. Campagna, P. Belser, A. von Zelewsky, Coord. Chem. Rev. 84 (1988) 85.
[62] K. Kalyanasundaram, Photochemistry of Polypyridine and Porphyrin Complexes, Academic Press, New York, 1992.
[63] W. Humbs, J. Strasser, H. Yersin, J. Luminescence 72–74 (1997) 677.
[64] J. Westra, M. Glasbeek, Chem. Phys. Lett. 166 (1990) 535.
[65] J. Westra, M. Glasbeek, Chem. Phys. Lett. 180 (1991) 41.
[66] M. Kato, S. Yamauchi, N. Hirota, Chem. Phys. Lett. 157 (1989) 543.
[67] H. Yersin, D. Braun, Coord. Chem. Rev. 111 (1991) 39.
[68] H. Yersin, J. Strasser, J. Luminescence 72–74 (1997) 462.
[69] H. Yersin, H. Otto, G. Gliemann, Theor. Chim. Acta (Berlin) 33 (1974) 63.
[70] M. Stock, H. Yersin, Chem. Phys. Lett. 40 (1976) 423.
[71] D. Trümbach, PhD-Thesis, Universität Regensburg, 1995.
[72] H. Yersin, D. Trümbach, J. Strasser, H.H. Patterson, Z. Assefa Inorg. Chem. 37 (1998) 3209.
[73] H. Yersin, D. Braun, D. Trümbach, in: G. Calzaferri (Ed.), 10th Intern. Conf. on Photochem. Conversion and Storage of Solar Energy (IPS 10), Book of Abstracts, 1994, p. 319.
[74] G.I. Kerley, High-Pressure Sci. Technol., Am. Inst. Phys. AIP, Conf. Proc. 309 (1993) 903.
[75] P. Loubeyre, R. LeToullec, High Pressure Research, vol. 3, Gordon and Breach Science, New York, 1990, p. 263.
[76] H. Yersin, D. Donges, Transition Metal and Rare Earth Compounds - Excited States, Transitions, Interactions, in: H. Yersin (Ed.), Topics in Current Chemistry, Springer, Germany, (2000) in press.
[77] H. Wiedenhofer, PhD-Thesis, Universität Regensburg (1994).
[78] H. Backert, H. Yersin, A. von Zelewsky, 13th Intern. Symp. on Photochem. and Photophys. of Coordination Compounds, Lipari 1999. Book of Abstracts p. 90.
[79] M. Eichenseer, Diplomarbeit, Universität Regensburg (1999).
[80] P. Huber, H. Yersin, J. Phys. Chem. 97 (1993) 12705.